

AD-755 282

ELECTRICAL CHARGING OF A CYLINDER BY A
SEEDED VORTEX

Philip B. Bohl, et al

Ohio State University

Prepared for:

Army Research Office-Durham

October 1972

DISTRIBUTED BY:

NTIS

National Technical Information Service
U. S. DEPARTMENT OF COMMERCE
5285 Port Royal Road, Springfield Va. 22151

AD755292-4942-20-E

AD755292

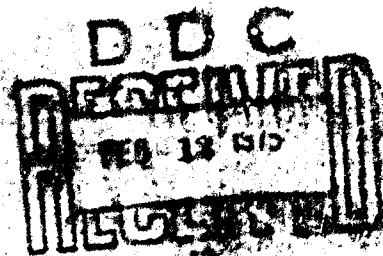
ELECTRICAL CHARGING OF A CYLINDER BY
A SEEDED VORTEX.

Philip B. Bohl
H. R. Velkoff

Inceris Technical Report #15
Contract DA-31-124-ANO-D-246

U. S. Army Research Office - Durham
Box 04, Duke Station
Durham, North Carolina 27706

October 1972



The Ohio State University Research Foundation
Columbus, Ohio 43212

Approved for public release; distribution
unlimited.

DISCLAIMER

The findings in this report are not to be construed as an official Department of the Army position unless so designated by other authorized documents.

The citation of trade names and names of manufacturers in this report is not to be construed as official Government endorsement or approval of commercial products or services referenced.

Best Available Copy

Unclassified

Security Classification

DOCUMENT CONTROL DATA - R & D

(Security classification of title, body of abstract and indexing annotations must be entered when the overall report is classified)

1. ORIGINATING ACTIVITY (Corporate author) The Ohio State University Research Foundation 1314 Kinnear Rd., Columbus, Ohio 43212		2a. REPORT SECURITY CLASSIFICATION Unclassified	
		2b. GROUP N/A	
3. REPORT TITLE ELECTRICAL CHARGING OF A CYLINDER BY A SEEDED VORTEX			
4. DESCRIPTIVE NOTES (Type of report and inclusive dates) Interim Technical Report			
5. AUTHOR(S) (First name, middle initial, last name) Philip B. Bohl, H. R. Velkoff			
6. REPORT DATE October 1972		7a. TOTAL NO. OF PAGES 100/105	7b. NO. OF REFS 16
8a. CONTRACT OR GRANT NO. DA-31-124-ARO-D-246		8b. ORIGINATOR'S REPORT NUMBER(S) Technical Report # 15	
b. PROJECT NO. 20010501B700		9b. OTHER REPORT NO(S) (Any other numbers that may be assigned this report) AR00-4942-20-E	
c. 1D12140A142			
10. DISTRIBUTION STATEMENT Approved for public release; distribution unlimited.			
11. SUPPLEMENTARY NOTES		12. SPONSORING MILITARY ACTIVITY U. S. Army Research Office - Durham Box CM, Duke Station Durham, North Carolina 27706	
13. ABSTRACT It is a well established fact that aircraft, especially helicopters, become electrically charged in particular conditions of flight, such as in the case of flying or hovering near particulate matter. The trailing vortices shed by each rotor tip, in the case of a helicopter, flow downward in a helical path and bathe the surface of the helicopter with the fluid field associated with the vortex. The purpose of this research work was to measure the electrical charging rate of a cylindrical body bathed by the trailing vortex shed by a differential airfoil "seeded" with charged particulate in a subsonic wind tunnel. It was found that the charging rate increased directly with the wind tunnel speed. As the angle of attack for the differential airfoil was increased, making a larger diameter vortex, the charged particles were thrown out farther from the center of the vortex. The charging rate on a cylindrical body placed at the center of the vortex was decreased. An airfoil wetted with water was found to reduce the charging rate on the metal cylinder. The electrical field of the wooden test cylinder increased with an increase in the wind tunnel speed.			

Unclassified

Security Classification

14	KEY WORDS	LINK A		LINK B		LINK C	
		ROLE	WT	ROLE	WT	ROLE	WT
	Electrofluidmechanics Electrohydrodynamics Electrogasdynamics Electrostatic (Electrostatic Charging) Charged Particle Vorte. Fluid Mechanics Helicopter Charging Static Charging						

Unclassified

Security Classification

ELECTRICAL CHARGING OF A CYLINDER BY
A SEEDED VORTEX

Philip B. Bohl

H. R. Velkoff

Interim Technical Report #15

Contract DA-31-124-ARO-D-246

U. S. Army Research Office - Durham
Box CM, Duke Station
Durham, North Carolina 27706

October 1972

The Ohio State University Research Foundation
Columbus, Ohio 43212

Approved for public release; distribution
unlimited.

FOREWORD

The work reported herein was sponsored in part by the United States Army Research Office, Durham, under Contract No. DA-31-124-ARO-D-246. The study presented herein was conducted by Mr. Philip B. Bohl in fulfilling the requirements for a thesis in his Master of Science program at The Ohio State University.

ABSTRACT

It is a well established fact that aircraft, especially helicopters, become electrically charged in particular conditions of flight, such as in the case of flying or hovering near particulate matter. The trailing vortices shed by each rotor tip, in the case of a helicopter, flow downward in a helical path and bathe the surface of the helicopter with the fluid field associated with the vortex. The purpose of this research work was to measure the electrical charging rate of a cylindrical body bathed by the trailing vortex shed by a differential airfoil "seeded" with charged particulate in a subsonic wind tunnel.

It was found that the charging rate increased directly with the wind tunnel speed. As the angle of attack for the differential airfoil was increased, making a larger diameter vortex, the charged particles were thrown out farther from the center of the vortex. The charging rate on a cylindrical body placed at the center of the vortex was decreased. An airfoil wetted with water was found to reduce the charging rate on the metal cylinder. The electrical field of the wooden test cylinder increased with an increase in the wind tunnel speed.

ACKNOWLEDGEMENT

The author wishes to express his appreciation to Professor H. R. Velkoff of The Ohio State University for his guidance and assistance throughout the research project upon which this thesis is based.

TABLE OF CONTENTS

	<u>Page</u>
ABSTRACT	iii
ACKNOWLEDGEMENT	iv
LIST OF TABLES	vii
LIST OF ILLUSTRATIONS	viii
CHAPTER	
I. INTRODUCTION	1
II. LITERATURE REVIEW	3
III. TEST EQUIPMENT	11
3.1 Wind Tunnel	11
3.2 Particulate Feed and Filter System and Particulate	13
3.3 Differential Airfoil	15
3.4 Cylindrical Test Body	16
3.5 Electrical Circuit Instrumentation	18
3.6 The Electrical Field Mill	23
IV. EXPERIMENTAL RESULTS	24
4.1 "Wetted Airfoil Phenomenon"	24
4.2 Metal Cylinder Testing	26
4.3 Charge Generation	27
4.4 Tests to Conduct	30
4.4.1 PART I - Electrical Current Measurements for the Copper Cylinder Using the Wood Airfoil	33
4.4.2 PART II - "Wetted Airfoil Phenomenon" Tests	33

Table of Contents (cont.)

	<u>Page</u>
4.4.3 Procedure for Measuring Charging Currents .	34
4.4.4 PART III - Electrical Field Mill Tests . .	35
4.5 Data from Experimental Results	36
V. DISCUSSION OF RESULTS	61
VI. CONCLUSION	67
VII. RECOMMENDATIONS	69
BIBLIOGRAPHY	71
APPENDICES	
I. WIND TUNNEL CALIBRATION DATA	73
II. POLY-VINYL-CHLORIDE INFORMATION	76
III. PHOTOGRAPHS AND WIRING DIAGRAM OF EXPERIMENTAL SET-UP	78
IV. OPERATION OF THE ELECTRICAL FIELD MILL	85

LIST OF TABLES

<u>Table</u>		<u>Page</u>
I	Cloud Charge Produced for Materials Blown Through a Brass Tube	6
II	Precipitation Charging	7
III	Charging Current and Voltages for Aircraft in Clear Air	8
IV	Cylinder Charging Rates	27
V	Air Supply Settings	32
VI	Tunnel Speed vs. Charge at Inlet Screen	32
VII	Wind Tunnel Speed	36
VIII	Location of Test Body	37
IX	Velocity Correction Factors for Non-Standard Ambient Pressure and Temperature	75
X	Physical Properties of Poly-Vinyl-Chloride (PVC)	77
XI	PVC Sieve Analysis Results	77

LIST OF ILLUSTRATIONS

<u>Figure</u>		<u>Page</u>
1	Wind Tunnel	12
2	Low Pass Filter	20
3A	Typical Charging Rate - No Filter	21
3B	Typical Charging Rate - Filter	21
4	Non-Filtered Brush Strip Chart Recording	22
5	Charge Generation Diagram	31
6	Differential Airfoils	37
7	No Airfoil, Location	38
8	No Airfoil, Centerline	39
9	$\pm 0^\circ$ Wood Airfoil, Location	40
10	$\pm 0^\circ$ Wood Airfoil, Centerline	41
11	$\pm 7^\circ$ Wood Airfoil, Location	42
12	$\pm 7^\circ$ Wood Airfoil, Centerline	43
13	$\pm 12^\circ$ Wood Airfoil, Location	44
14	$\pm 12^\circ$ Wood Airfoil, Centerline	45
15	Centerline Charging Rates Compared for Angles of Attack for Wood Airfoil	46
16	3 Diameters Above Centerline (3 DU), Angles of Attack	47
17	Typical Charging Range	48
18A	Brush Recorder Output - $\Delta P = 4''\text{H}_2\text{O}$	49
18B	Brush Recorder Output - $\Delta P = 1''\text{H}_2\text{O}$	49
19	Distance From Airfoil	50

List of Illustrations (cont.)

<u>Figure</u>		<u>Page</u>
20	Frequency of Counts at Current Levels	51
21	Probability Plot for Frequency of Counts	52
22	Wetted Wood Airfoil, Centerline	53
23	Charging Rate for Aluminum Foil Airfoil and Copper Cylinder, $\pm 0^\circ$	54
24	Charging Rate for Aluminum Foil Airfoil and Copper Cylinder, $\pm 7^\circ$	55
25	Charging Rate for Aluminum Foil Airfoil and Copper Cylinder, $\pm 12^\circ$	56
26	Charging Rate for Oil on Aluminum Foil Airfoil	57
27A	Typical Field Mill Traces - Field Mill Alone	58
27B	Typical Field Mill Traces - Field Mill in Wood Cylinder	58
28	Electrical Field Mill Output, Location	59
29	Electrical Field Mill Output, Centerline	60
30	Average Velocity Entering Test Section	74
31A	Air Speed Adjustment Doors	79
31B	Particle Hopper and Nozzle	79
32A	Inflated Filter Bag	80
32B	Differential Airfoils	80
33A	Metal Cylinder in Holding Fixture at Centerline Position	81
33B	Wooden Cylinder in Holding Fixture with Electrical Field Mill	81

List of Illustrations (cont.)

<u>Figure</u>		<u>Page</u>
34A	Electrical Field Mill and Wooden Cylinder	82
34B	Electrical Field Mill Inserted in Wooden Cylinder	82
35	Electrical Equipment Set-Up	83
36	Wiring Diagram of Test Instrumentation	84
37	Gaussian Surface	85
38	Field Mill Head Section	88
39	Electrical Field Mill Calibration	90
40	Field Mill Calibration Set-Up	91

I. INTRODUCTION

The exact phenomenon of how a helicopter becomes electrically charged while in flight is still an unanswered problem that researchers are trying to determine. Although, it is a well established fact that aircraft, especially helicopters become electrically charged in particular conditions of flight, such as in rain, hail, or near particulate matter as in the case of flying or hovering over dusty terrain. Various theories for determining the method of static charging to the aircraft have been speculated. Some researchers attribute the charging to ions in the exhaust gases, to precipitation charging occurring when particles in the air (water droplets, dust, or snow) impact the surface of the aircraft, and to the movement of the aircraft through varying electrical fields present in the atmosphere.

The static charging of a helicopter is important because of its effect on the safety of personnel and cargo. The helicopter may discharge through loading slings as it hovers for loading and unloading of cargo or for some sort of a rescue operation. The resulting discharge may cause painful electrical shocks to the loading personnel or it may present a serious fire or explosion if flammable or explosive material is located near the loading or unloading site.

Another problem associated with the electrical charging of aircraft is communication interference. An electrical field is set up around the charged aircraft which may discharge some of the charge on the aircraft at "sharp" points on the aircraft by the process of corona discharge. The corona discharge currents are electrically

noisy. They produce so much static noise that communication signals are wiped out (1).

While the trailing vortices shed from the tips of fixed wing aircraft flow downstream behind the aircraft and become dissipated in the atmosphere, the trailing vortices shed by each rotor tip in the case of a helicopter flow downward in a helical path and bathe the surface of the helicopter with the fluid field associated with the vortex. The purpose of this research work was to measure the electrical charging rate of a body bathed by the trailing vortex shed by a differential airfoil "seeded" with charged particulate.

The investigation was conducted in a low turbulence subsonic wind tunnel. A conducting cylindrical object was placed downstream of the airfoils to collect the charged particulate distributed throughout the trailing vortex. The charging rate at various wind tunnel speeds was measured for different positions of the cylindrical object with respect to the vortex center. Tests were also made on conducting and non-conducting airfoils to determine their effects on the charging rate. A non-conducting body replaced the conducting cylindrical object so that the electrical field in the vortex could be measured.

II. LITERATURE REVIEW

A discussion of the previous work done concerning the subject of trailing vortex properties such as pressure and velocity distribution and decay of the vortex strength are unnecessary here, since the object of this research was confined to electrical charging of a body placed in a vortex. Only that information dealing with vortex charging and static electrification will be cited in this review.

Daugherty (2) conducted research to study the charge generating and separation capabilities of a trailing vortex system and to determine if the trailing vortex system could create a stable electrical field. His research was carried out with the same experimental set-up as used in this research. A description of this set-up will be given in Chapter III. A particle impact probe was used to determine the particle density distribution and an indication of the particle charge. Results of Daugherty's research indicated that the trailing vortex system in a flow seeded with particles did establish a quasi-static electrical field distribution due to the electrostatic charge which resided on the swirling seeded particles. The particle charge increased with increase in the angle of attack of the airfoils; the increase in charge was proportional to the increase in the maximum tangential velocity of the trailing vortex.

Observation by Lavan and Fejer (3) of luminescence in supersonic swirling flow were made during vortex tube experiments. When a dielectric test section was used in combination with a Mach 2 nozzle and with relatively high swirl velocities, the central region of the flow

became luminescent. The luminescence occurred only for a dielectric test section rather than a conducting test section. Also, the charging mechanism was attributed to the condensation of the humid air. Water droplets formed in the supersonic nozzle during the rapid expansion of the humid air were entrained by the swirling flow entering the test section. The smaller droplets were on the average negative, while the larger ones carried statistically a positive charge. The centrifugal flow field resulted in an accumulation of positive charges on the wall; thus, there was a charge separation mechanism that took place which left the negatively charged droplets near the center of the test section and placed the positively charged particles at the wall of the test section. When the intensity of the field reached a certain level, glow discharge ensued.

When particles strike an aircraft in the atmosphere, a precipitation charge may develop due to one, or a combination of the following, basic mechanisms: frictional electricity, electrolytic electricity, spray electricity, and contact or voltaelectricity. A description of these basic mechanisms will be given to enlighten the reader on the subject of generating static electricity.

Frictional electricity (4) occurs when two dry materials with different dielectric constants (non-metals) come into contact with each other and then separate; the material with the largest dielectric constant will be charged positively. It is believed that electrification is a result of the exchange of molecular ions. This phenomenon is very complicated since changes in the structure of the surface, such as in a film of oil, have great effects on the generated voltages.

Spray electricity (4) occurs when the disruption of surface liquid film by mechanical force causes the electrical double layer to break (for example, water; outside negative, inside positive). This results in the separate parts having dissimilar charges and hence causes static charge build-up.

Electrolytic electricity (4) is produced in solutions of liquids of high dielectric constant by a distribution of electrolytic ions between the solutions and the metal or solid. This diffusion of ions can build up large potentials.

Contact or voltaelectricity (4) occurs when two clean surfaces of metals or semiconductors come into contact with each other. The metal with the higher work function will become positive because more electrons diffuse from that metal to the metal of the lower work function. The resulting voltages are small. Additional information concerning contact charging can be found from Harper (5).

The following experimental data will give some idea of the effect of electrification of dusts on dispersion and impact on surfaces. The charging is brought about by surface contact of the various substances with each other.

Table I gives the results of experiments conducted by Whitman (6) for blowing various dust materials through a brass tube.

Table I

Cloud Charge Produced For Materials Blown Through a Brass Tube

Dust Material	Weight (g)	Charge on Cloud (C/kg)
Borax	0.15	-3.3×10^{-6}
Sodium bicarbonate	0.17	4.0×10^{-6}
Lime	0.07	3.8×10^{-6}
Fused Quartz	0.13	-2.9×10^{-6}
Ammonium Chloride	0.19	-3.4×10^{-6}
Sodium Carbonate	0.12	-2.3×10^{-6}
Sodium Fluoride	0.13	1.7×10^{-6}

Experiments reported by Kunkel (7) show that with time, micron sized particles whether initially charged or not acquire equilibrium Gaussian charge distribution by interaction with atmospheric ions. A special gun was designed to yield puffs of dust samples of uniform assorted and controlled magnitude. Results of his tests indicated that when contact of the same substance occurred (such as blowing sulfur out of sulfur, or quartz out of quartz) the number of positive and negative particles was about equal, thus, giving symmetrical charging. The most pronounced case of asymmetrical charging was for quartz blown out of a sulfur duster. In this case the quartz retained a negative charge, and when the sulfur was blown out of quartz, there was indicated a positive charge on the dust.

Concerning the charging of aircraft, the sign of the charge on the plane, for example, (1) has been known to change as a result of servicing and the wiping of the plane surfaces with greasy rags. It was also found possible to discharge the plane by letting water run out of its trailing edges. The amount of water needed was

prohibitively great.

The charging rate at which the aircraft is charged, with no discharge mechanism present, depends on the material, mass, and charge intercepted. The amount of charge present on the aircraft is a function of the total amount of precipitation intercepted. Hence, the bigger the aircraft, or larger the surface area, and the faster the speed, the larger the amount of charge collected by the aircraft in flight.

To give the reader some appreciation of the charge developed on a helicopter from precipitation charging, Table II is presented (8).

Table II
Precipitation Charging

Type	Charge Developed on an Aircraft $C = 200 \mu\text{MF}$
Quiet Rain	+0.3 to -0.5 KV/sec
Shower Rain	+10 to -10 KV/sec
Electrical Storm Rain	+21 to -13 KV/sec
Quiet Snowfall	+0.1 to -0.1 KV/sec
Squall Snowfall	1.5 to -0.8 KV/sec
Dirt	+5 to +13 KV/sec
Fuel Drops	-4 to -38 KV/sec

Table III gives the charging current and voltage for particular aircraft (9) in clear air conditions.

Table III

Charging Current and Voltages for Aircraft in Clear Air

Aircraft	Height above Ground (ft)	Time Since Last Earthed(sec)	Charging Current (μ A)	Voltage (KV)
Wessex 5	20	90	+0.05	6
Belvedere	20	60	+0.4	+2.0
Whirlwind 10	20	90	+0.7	+48.0
Whirlwind 10	20	120	+0.6	+52.0

Although this research project is not concerned with discharging the aircraft, rather it is to study charging phenomenon, some information dealing with present day discharging methods of aircraft may be of interest to the reader. Presently, in flight electrical discharges are confined to various corona dischargers. The corona points give off corona discharge currents at a sufficiently high voltage so that the ions formed are blown away from the aircraft by the slipstream (10). Discharges may be classified into passive and active types; the passive type operates by virtue of the voltage of the aircraft itself relative to the surroundings, while the active type is connected to a high voltage power supply so that it can discharge substantial current even when the aircraft as a whole is at a low voltage. Usually, the passive type is adequate in controlling the radio interference effects of electrostatic charge, and is therefore sufficient for fixed wing aircraft where this is the main problem. Helicopters, however, present hazards to personnel and to

sensitive stores, when they are hovering and an electrical connection is made to ground, and moreover the airflow for charge dispersal is less than that of the fixed wing aircraft. Therefore, active dischargers for helicopters have been given much attention (10).

Daugherty (2) using the approaches taken by Soo (11) and Hirschken developed a computer program to determine the path of an individual particle as it passed over the airfoils and into the trailing vortex system. This program simulated the interaction of the particle with the flow field including a three dimensional path of each particle using Newton's laws of motion. The only force considered to be acting on the particle motion was the drag force on each particle due to the relative motion with the fluid. Gravitational, electrical, and magnetic forces were excluded.

Results of this math model showed that particles initially near the vortex center were thrown out of the vortex core and that their trajectories intersected the trajectories of particles initially outside the vortex core. The larger diameter particles moved radially outward faster than the smaller diameter particles. From the results, Daugherty (2) suggested two mechanisms whereby a trailing vortex system acted as a charge separator and a charge generator. The charge separation mechanism was brought about through separation of particles to the outside of the vortex core. The charge generation occurred through particle - particle interactions which increased the charge level of the particle.

Daugherty (2) continued to give expressions for the electrical field set up in the vortex. From his experimental results, he showed

that contours of constant electrical field strength were approximately circular, and that the electrical field increased approximately linearly along a radius from the vortex core. Daugherty's numerical solutions for the electrical field expression indicated that an individual particle trajectory was not altered by the electrical field set up by the neighboring particle.

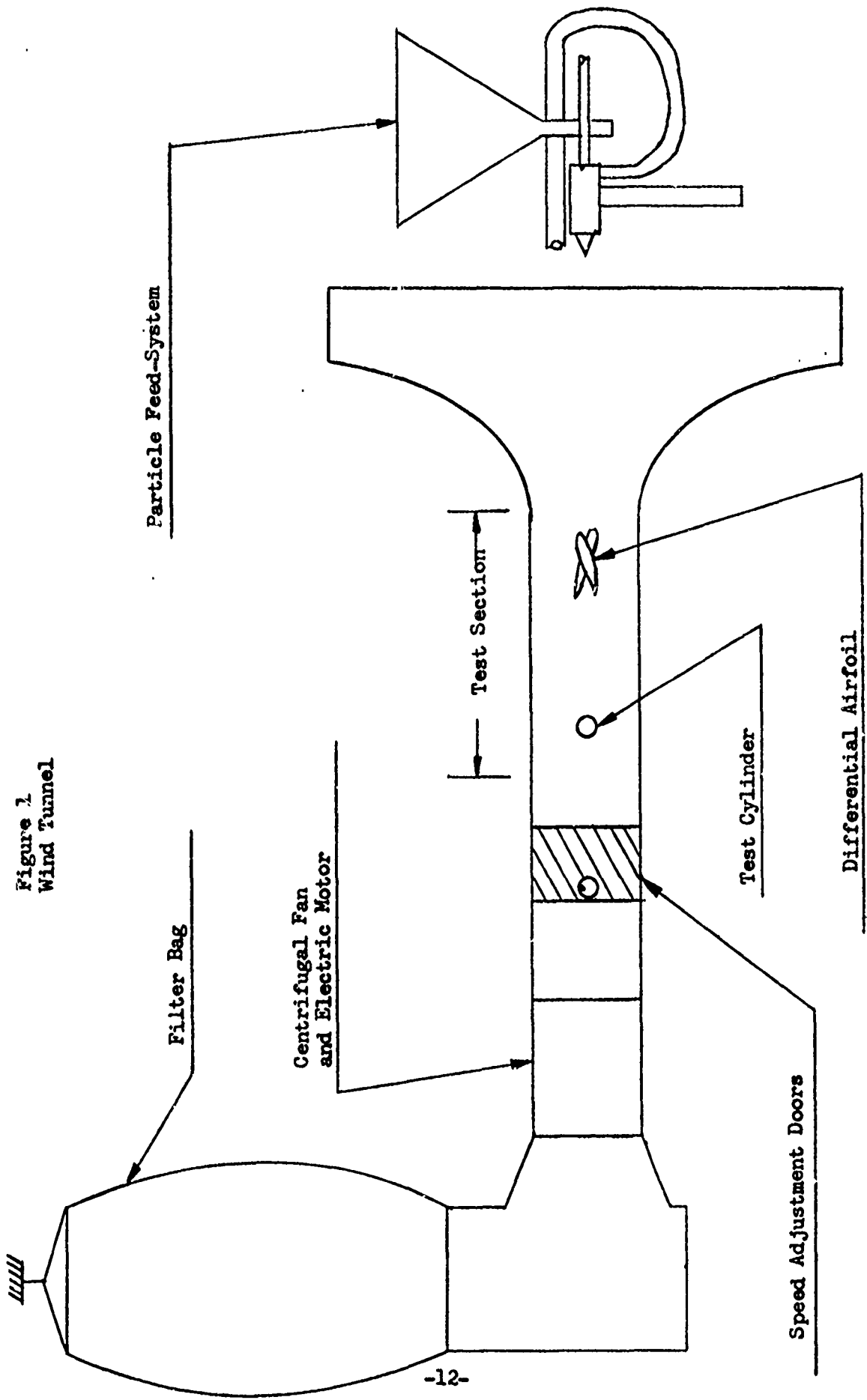
III. TEST EQUIPMENT

3.1 Wind Tunnel

The test equipment used in this research is described in detail by Daugherty (2) who used the same wind tunnel and associated hardware for his research. Consequently, only a brief description of the components used in this research will be given.

Figure 1 was included in this description to familiarize the reader with the experimental set-up. The wind tunnel used in this work was a low-turbulence subsonic variety capable of developing test section velocities of 187 ft./sec. It was designed and constructed by Diller (12). The inlet section contained three damping screens, two of which were removed for this research to allow less restriction for the particulate flow. A constant speed motor and centrifugal fan were used to power the wind tunnel. Downstream from the test section, a set of hinged doors were opened or closed by a small hand crank to allow varying amounts of air to be drawn from the test section (2). See Appendix III, Figure 31A. When the doors were fully opened, they were flush with the sides of the wind tunnel and allowed air to be drawn only from the test section. As the doors were closed somewhat, they blocked off air coming from the test section, but at the same time they allowed air to be drawn from outside the wind tunnel test section. Thus, the fan always drew the same amount of air, but by adjusting the hinged door varying amounts of air could be drawn from the test section. A manometer

Figure 2
Wind Tunnel



U
S
N
A
V
Y
A
R
M
Y
A
I
R
F
O
R
C
E
C
O
S
T
A
L
M
A
R
I
N
E
S
E
R
V
I
C
E

was located near the hinged door and hand crank so that the pressure drop between the inlet of the test section and the atmospheric pressure could be noted. The wind tunnel was calibrated previously by Diller (12). See Appendix I for calibration information. Removable doors were located in the test section to install and relocate test equipment in the wind tunnel test section.

The test section was thirteen feet long and one and one-half by two feet in cross section. It was constructed from 3/4 inch plywood with the inside coated with ten coats of non-pigmented varnish in order to obtain good dielectric properties for the tunnel wall (2). The inside corners of the tunnel were filleted with 3/8 inch wood moldings.

3.2 Particle Feed and Filter System and Particulate

The wind tunnel flow field was seeded with particles which were blown into the wind tunnel inlet screen. Daugherty (2) designed a particle feed system operated by an external air supply line. The particles were stored in a spring-loaded hopper capable of holding fifty pounds of particles. The spring-loaded hopper operated a dial indicator that indicated the weight of the particles in the hopper. Thereby, the particle flow rate was determined by recording the difference in hopper weights over a certain timed interval. See Appendix III, Figure 31B. The spout of the hopper was connected to the throat of a venturi. Air was fed to the venturi by the external air supply. Air passing through the venturi mixed with the particles from the hopper and carried them into a mixing chamber in the particle feed nozzle.

The nozzle, which directed the particles against the wind tunnel inlet screen, consisted of a cylindrical mixing chamber section, a converging-diverging section, and a hollow sting running down the center of the nozzle. At the end of the sting was a hollow deflecting cone. The mixing chamber received the mixture of air and particles from the hopper section and also unseeded air from the air supply. This mixture was exhausted through the converging-diverging section toward the wind tunnel inlet. A third air supply line was attached to the hollow sting. Air passing through the sting was exhausted through air jets located in the base of the deflecting cone. This helped reduce core velocity of the nozzle and helped shape the nozzle exhaust plume. See Daugherty (2) for details.

A filter system was developed to prevent particles from blowing throughout the laboratory so they could be reused for more tests. Daugherty (2) attached a large eighteen foot high by twelve foot diameter filter bag made of cotton flannel to the turning box at the wind tunnel exit. See Appendix III, Figure 32A for inflated filter bag. The filter bag was suspended from a circular hoop attached to the laboratory ceiling. The inside of the filter bag had a heavy nap which trapped the particles. After several test runs, the filter bag was agitated to release the trapped particles so that air could escape through the pores of the fabric.

The particulate flow was used to simulate the way helicopters become electrically charged by flying or hovering in a region of particulate, such as in dusty terrain. Daugherty (2) experimented

with various types of particles, such as petro sand, glass beads, and poly-vinyl chloride resin. Most of his experimental work involved the use of poly-vinyl chloride which seemed to become charged more noticeably than the other particles, and it was not as corrosive to the wind tunnel as the sand or glass. The experiments conducted throughout this research involved the sole use of poly-vinyl chloride. Poly-vinyl chloride particles are spherical in shape, white in color, and chemically inert. Appendix II gives the physical properties and sieve analysis performed by Daugherty (2) for the poly-vinyl chloride resin.

3.3 Differential Airfoil

The differential airfoil was two airfoil sections of equal span length and chord length which were mounted tip to tip across the wind tunnel test section. The airfoil sections were positioned so that the angle of attack of one section was equal and opposite to that of the other section. See Appendix III, Figure 32B. The airfoils were supported in the wind tunnel at their quarter-chord position by a steel support rod which held the airfoils securely in any predetermined angle of attack. The airfoils were located at a set of removable plexiglass doors in the test section. Transparent angle of attack indicators were taped to the moveable doors. The angle of attack was determined by merely reading where the center of the airfoil lined up with the transparent angle of attack indicator. A differential airfoil proved to be useful in this work because it

produced a stable vortex whose position in the wind tunnel was independent of flow velocity, airfoil angle of attack, and distance downstream from the airfoils. The airfoils were made of bass wood for the trailing edge and birch wood for the leading edge. The pieces were glued together and the surfaces were sanded smoothly to conform to the O012 airfoil shape. The airfoils were painted with non-pigmented varnish to improve the dielectric properties of the wood. See Daugherty (2) for details.

3.4 Cylindrical Test Body

A cylindrical test body was chosen to pick off the electrical currents produced by the charged particles in the vortex. The test body was moved across the vortex so that the electrical charging rate could be determined for various locations of the test body with respect to the center of the vortex. A two inch diameter copper tube was chosen as the test body. The diameter of the test body was selected by taking into account the size of the vortex downstream of the differential airfoil and the cross-sectional area of the wind tunnel. A location of six feet downstream of the airfoils resulted in a visible ring of white particles approximately one foot in diameter for a ± 12 degree angle of attack for the airfoils. Visualization of the particles was brought about by placing a bright light at one of the removable plexiglass doors in the test section. Observations of this particulate ring were made at the tunnel inlet looking into the tunnel, with the wind tunnel fan

turned on and the particle feed system in operation. The two inch diameter cylinder when placed in a horizontal position was able to travel vertically in the wind tunnel three diameters above and below the centerline position to cover the one foot diameter ring of particulate. In increments of one diameter of the test cylinder, seven positions of the test cylinder were used to measure the electrical charging rate in the seeded vortex. These increments were 3 diameters above centerline to 3 diameters below centerline in increments of one diameter. Since the cross-sectional height of the test section was two feet, the effect of the wall boundary layer was assumed not to affect the air flow for the test cylinder in its positions closest to the wall because there still remained five inches of clearance between the test cylinder and the wind tunnel upper or lower wall.

To conduct the electrical field tests, a dielectric material was used for the test cylinder, so that the field mill could be used to measure the electrical field in the test body. A two inch diameter soft pine wood cylinder was turned down on a lathe so as to be comparable in dimension to the copper tube. This wooden cylinder was covered with two coats of exterior varnish. A 7/8 inch diameter hole was bored through the surface of the cylinder so that the front end of the field mill could be placed in the wooden cylinder to measure the electrical field. Section 3.6 and Appendix IV give details on the electrical field mill.

A holding fixture was constructed to hold and position the copper and wooden cylinders in the test section of the wind tunnel. The holding fixture was constructed so that the cylindrical test bodies could be traversed vertically in the test section as well as longitudinally along the test section. A minimal size requirement was used so that sufficient air flow could be established through the test section. Also, it was desirable to have the holding fixture designed so that it would not affect the electrical field measurements for the wooden cylinder. The holding fixture was constructed of soft pine not coated by any substance to improve its dielectric properties, thus making a definite boundary between the test section wall and the test body. The holding fixture consisted of three square wooden blocks, three and one-half inches a side, one on each end of the test cylinder and the other one wedged to one side of the test wall by drawing two wooden wedges together by a single bolt. Appendix III, Figures 33 and 34 show photographs of the metal cylinder and wooden cylinder in the test section as well as the electrical field mill and how it was positioned in the wooden cylinder.

3.5 Electrical Circuit Instrumentation

This section deals with instruments used in measuring the electrical charging rate on the copper tube placed downstream of the seeded vortex. First of all, the order of magnitude of the charging had to be determined for the seeded vortex flow on the metal cylinder. A microammeter with 150 micro-amps full scale reading was connected

to the cylinder and ground and found to give a reading just greater than the zero reading on the meter, thus indicating about one-half a micro-ampere. A Keithley Model 303 D.C. Indicating Amplifier was then adapted to measure small currents by using a Model 3034 Decade Shunt, which converted the Keithley into a micromicroammeter for measuring currents as small as 10^{-12} ampere. The Keithley Model 303 D.C. Indicating Amplifier was a high gain electrometer voltmeter and D.C. amplifier for frequency ranges of D.C. to 100 KC. Accuracy was within one percent for the ranges being used for the micromicroammeter in this experiment. A built-in meter in the Keithley indicated the current being measured. The out-put of the Keithley amplifier was fed into a Tektronix Type 502A Dual-Beam Oscilloscope, which was used to observe the current signals from the coppertest cylinder. In the initial testing the current was read from the meter in the Keithley, although the needle of the meter oscillated considerably. Observation of the current in the oscilloscope indicated quite a random signal about a particular D.C. level of current. Since a D.C. level of current was desired for taking data, some sort of averaging of the oscillating current was necessary. A Brush Recorder Mark 280 strip chart recorder was connected to the output of the Keithley amplifier to record the current signal. Hopefully, with the Brush recorder an average of the recorded signal could be determined, but as it turned out the signal filled the entire width of paper with its wild oscillations, making an average approximation impossible to determine. A low pass filter (13) was

designed for cutting off frequency signals above two and one-half cycles per second. See Figure 2. Use of this filter resulted in a level signal with very few oscillations about the indicated D.C. current level.

Figure 2
Low Pass Filter

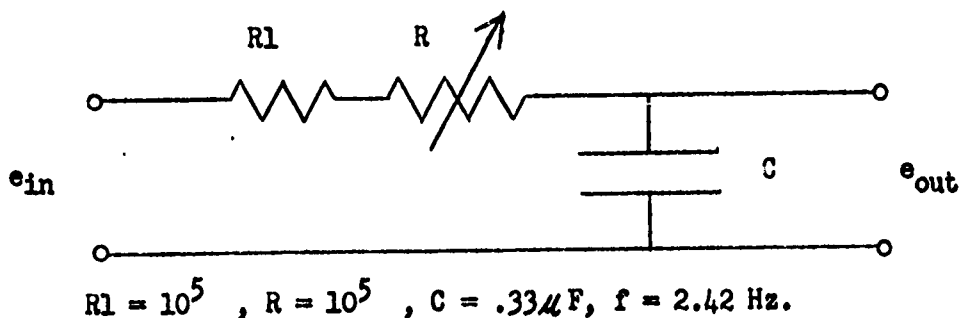


Figure 3 shows typical filtered and non-filtered oscilloscope traces for the current readings. Figure 4 shows a typical non-filtered signal recorded by the Brush strip chart recorder.

To obtain some information about the oscillation of the non-filtered current reading, the frequency of oscillations was taken for several current levels. This data was taken by use of the Monsanto Programmable Counter Model 110 B. The triggering level of the counter was found by connecting a digital voltmeter to the triggering level output pin of the Monsanto Counter. After the triggering level was determined, the counter recorded the number of oscillations about that particular current level.

Figure 3

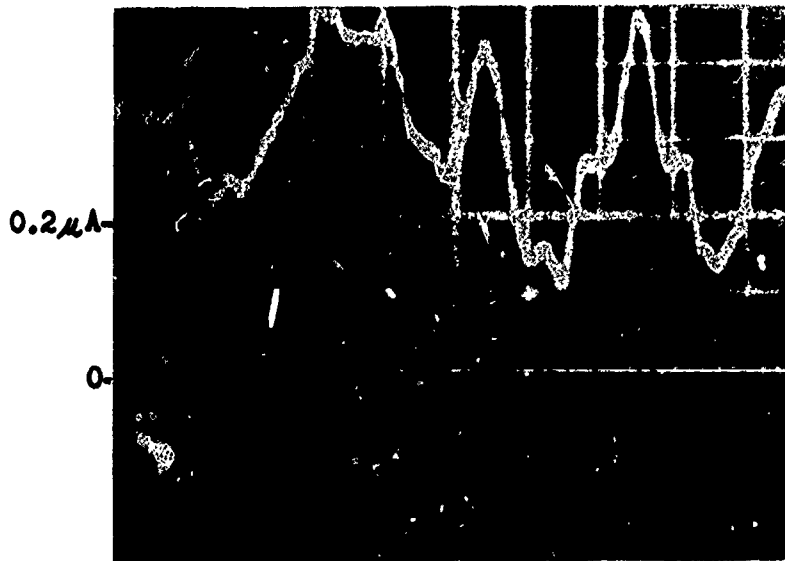
Typical Charging Rate on Copper Cylinder at Centerline

$\alpha = \pm 7^\circ$, Wood Airfoil, $\Delta P = 4''\text{H}_2\text{O}$

Oscilloscope Traces: $0.1\mu\text{A}/\text{cm}$; 5 m. sec./cm.

A

No Filter



B

Filter

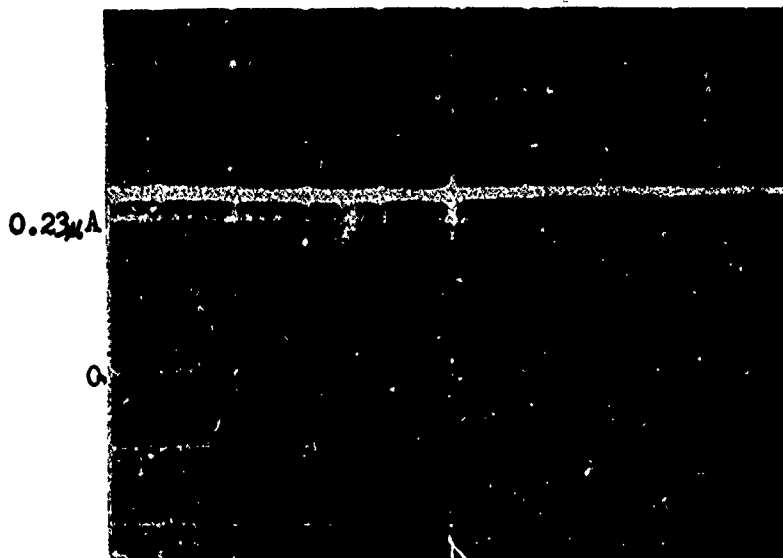
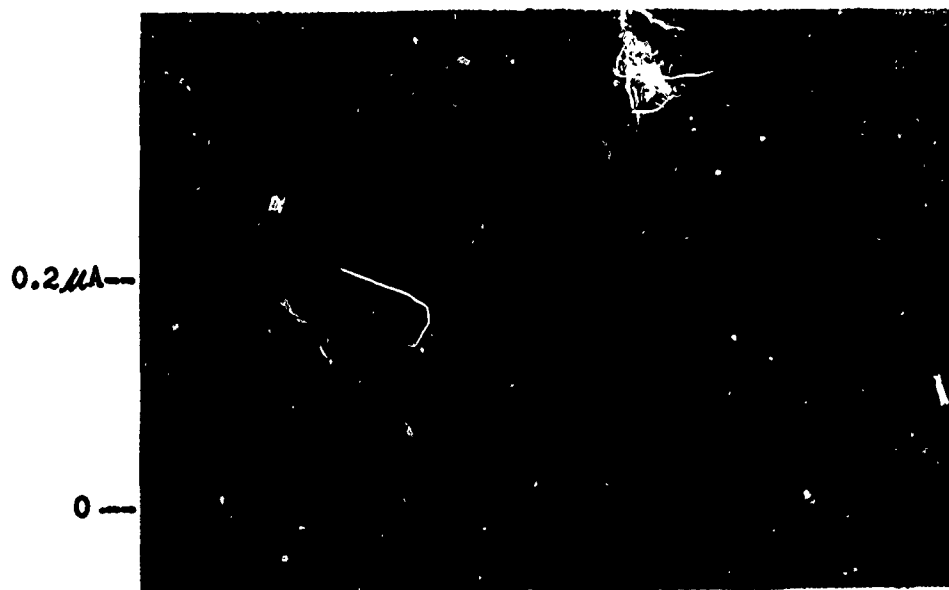


Figure 4
Non-filtered Brush Strip Chart Recording
Paper Rate: 200 mm./sec



A photograph of the electronic equipment used in this experiment and the wiring diagram for the electronic equipment set-up may be found in Appendix III, Figures 35, 36.

3.6 The Electrical Field Mill

An electrical field measuring device was designed and constructed by Evans (14). A small electrical motor rotated the screening vane, alternately exposing and covering the stator surface. A surface charge was induced on the stator in the presence of an electrical field. The output of the field mill was connected to the Tektronix Oscilloscope where a sinusoidal voltage was shown to be proportional to the electrical field being measured. Appendix IV provides a more detailed description of the operation of the electrical field mill.

IV. EXPERIMENTAL RESULTS

Introductory Remarks

Throughout this chapter on results, reference to the speed of the wind tunnel will be given. Rather than give the velocity of the wind tunnel in feet per second, the velocity will be given in inches of water pressure drop across the wind tunnel inlet. Appendix I shows the wind tunnel calibration curve and correction factor for ambient pressure and temperature. Although the ambient temperature and pressure were measured for each test, when correction factors were employed to the most severe condition to determine the wind tunnel velocity, a maximum of five percent error resulted between the true velocity and the velocity given for standard condition of temperature and pressure for the various pressure drops.

4.1 "Wetted Airfoil Phenomenon"

To determine the center of the vortex flow pattern generated by the differential airfoils, a stream of boron trifluoride gas was injected into the flow stream just a few inches upstream from the differential airfoils. This gas formed a dense white smoke when it reacted with the moisture in the air, thus giving a visual indication of the vortex center. The copper cylinder was placed at the centerline position of the wind tunnel at a location six feet downstream from the differential airfoils. With the airfoils crossed at various equal and opposite angles of attack, and the wind tunnel turned on, the smoke from the boron trifluoride gas hit

directly on the metal cylinder, oscillating about the centerline one or two inches at the most. The smoke was confined to a stream of no larger than three inches in diameter at the six foot location. Varying the wind tunnel speed had no visible affect on the position of the smoke stream. Therefore, the differential airfoil appeared to produce a stable vortex independent of axial location, wind tunnel speed, and airfoil angle of attack.

With the particle feed system in operation and the copper cylinder in position, a reduced current reading was detected each time the boron trifluoride gas was injected into the airfoil. As a matter of fact, the reduced current reading remained even after the gas was turned off. Cleaning of the metal cylinder did not alter the observation that the current was reduced after the gas had been turned off. Since the gas was injected upstream from the airfoil, the smoke came in contact with the airfoil surface, leaving an oily sticky residue film on the inner ends of the airfoils. After this residue was wiped clean from the airfoils, the charging rate to the metal cylinder returned to the rate occurring before the gas was turned on. This phenomenon of reduced charging when the airfoils became partially covered with the wet-oily residue will be referred to as the "wetted airfoil phenomenon." A series of tests were designed to study this effect with water and oil on the surface of the airfoil. The results of these tests will be discussed later.

4.2 Metal Cylinder Testing

While studying the charging rate on the metal cylinder, it was found that the charging rate decreased over a period of time for any particular location of the test cylinder. The fact that moisture may be brought into the air supply line which would help to discharge the charged PVC and initiate a reduced charging rate was theorized. To remove this moisture variable from the experiment, an air filter was installed in the air supply line to trap all the moisture and foreign matter. As it turned out, throughout the entire testing period no moisture or foreign matter was found in the filter, thus indicating evidence of a dependable clean air supply. Visual observation of the copper cylinder indicated that the PVC, poly-vinyl chloride particles had impacted on the copper cylinder and had left a very fine white film on the surface of the copper cylinder. This film was easily removed with emery cloth to give the copper cylinder a very clean and shiny surface. Rather than clean the cylinder after each test run, a search for another cylinder material that would not give a reduced charging rate over a period of time was conducted. First of all, a chrome cylinder of similar dimension as the copper cylinder was tried. After a period of time, it also received a white film over its surface which reduced its charging rate. Next, aluminum foil was wrapped around the copper cylinder. The aluminum foil acted similar to the chrome and again with time, its charging rate was reduced. Also, with the aluminum foil, impacting by the PVC particles weakened the foil and made it become

brittle, so that it would develop tears and break off after a few hours of impacting from the PVC. Finally, a carbon rod was used to measure the charging rate. The carbon rod gave such low current readings compared to the other cylinder tests, that a complete test run was not completed for the carbon rod. Table IV gives the results for these metal cylinder tests.

Table IV

Cylinder Charging Rates
 $\Delta P = 4''\text{H}_2\text{O}$, Cylinder at Centerline, $\alpha = \pm 7^\circ$

	Charging Rate
Copper Cylinder	0.3 μA to 0.15 μA after 3 hours
Chrome Cylinder	0.25 μA to 0.10 μA after 2 hours
Aluminum Foil Cylinder	0.25 μA to 10 μA after 2 hours
Carbon Rod	0.0020 μA

After reviewing the results of this testing, a decision was made to use the copper cylinder and polish it with emery cloth and steel wool after each test run. By this technique the effect of reduced charging rate with time was minimized because of the short time required for each test, approximately fifteen minutes.

4.3 Charge Generation

While conducting the tests, the question was asked, "what caused the PVC particles to become electrically charged?" Removing the differential airfoils changed the charging rate very little, indicating that the airfoils were not the source of the charge

generation. Interaction of the PVC particles with one another may leave some particles charged positively and others negatively, but the net charge of a sample would indicate no net change. Experiments conducted by Kunkel (7) gave insight to the general charging phenomenon. Kunkel's results for blowing quartz out of a sulfur duster indicated asymmetrical charging; in this case, the quartz remained negative and the sulfur became positively charged.

In the present tests, it was hypothesized that asymmetrical charging occurred with the PVC becoming positively charged and the aluminum nozzle housing being charged negatively because of their differences in dielectric strengths. Several tests were conducted to determine the charging at the nozzle by simply connecting the input lead from the Keithley amplifier to the nozzle. Results of the tests showed, as hypothesized, that the nozzle was indeed negatively charged. The charging rate at the inlet screen was also measured and found to be positively charged. The nozzle tests showed that frictional electricity was the phenomenon involved with this asymmetrical charging. Several weeks after the nozzle charging tests were conducted, the nozzle charging rate was again measured, but this time a positive current was measured. All this time the PVC remained positively charged and the cylinder charging rate remained the same. The answer to the question as to why a positive charge now existed rather than a negative charge as was previously measured was found. By gradually opening the air valve to the air

mixer line of the nozzle chamber, the charge rate on the nozzle would go from positive to negative.

The nozzle as described earlier had three rubber hoses leading to the mixing chamber. One air line went to the sting and cone at the end of the nozzle; another line coming from the venturi of the particle hopper contained a mixture of air and PVC; and the third air line went to the mixing chamber of the nozzle. The air was supplied at 80 psi to the three air lines, each having a separate valve for adjusting air flows. The air line leading to the venturi of the particle hopper was adjusted to give the maximum particle flow, which was 1.60 lbm./minute of PVC. The sting air flow helped to increase the size of the plume leaving the nozzle. The air line leading to the nozzle mixing chamber was used to mix the air with PVC and blow this mixture out of the nozzle. As the valve to the air line of the nozzle was opened, more air entered the nozzle and thus pushed out the PVC mixture faster. At some critical opening of this air line the velocity of the PVC moving across the nozzle was sufficient for frictional electricity to develop, therefore setting up the asymmetrical charging.

It was theorized that again asymmetrical charging took place at the aluminum venturi where the PVC entered the air stream, therefore giving a positive charge to the PVC particles. As the PVC mixture was transported to the nozzle mixing chamber through a rubber insulated hose, it retained its positive charge. Then, at some velocity, below the critical velocity, the positively charged

PVC particles impinged upon the nozzle leaving it positively charged. Above this critical velocity asymmetrical charging took place leaving the nozzle negatively charged and giving the PVC particles a positive charge as they left the nozzle. Figure 5 shows a diagram of the nozzle and associated air lines and how the charge is carried. Table V lists the results of the currents measured at the nozzle and inlet screen for various opening of the air line valve. It may be noted that all tests in this experiment were run for the air line opened 1 turn.

The charging rate on the metal cylinder was affected very little by opening the air line; a slight increase in charging was noted for increased opening of the air line. Another noticeable charging change occurred when the speed of the wind tunnel was decreased. The charge on the inlet screen decreased with the decrease in wind tunnel speed, as is shown in Table VI. The effect of the wind tunnel speed had no effect on the charging rate at the nozzle.

4.4 Tests to Conduct

This section will give a listing of the tests to be conducted in this experiment. Following recommendations from the research conducted by Daugherty (2), consultation from Velkoff (16), and earlier results found in performing the experiment, such as the "wetted airfoil phenomenon", a series of tests were designed and conducted to find the effect of the seeded vortex flowing over the cylindrical bodies.

Figure 5

Charge Generation Diagram

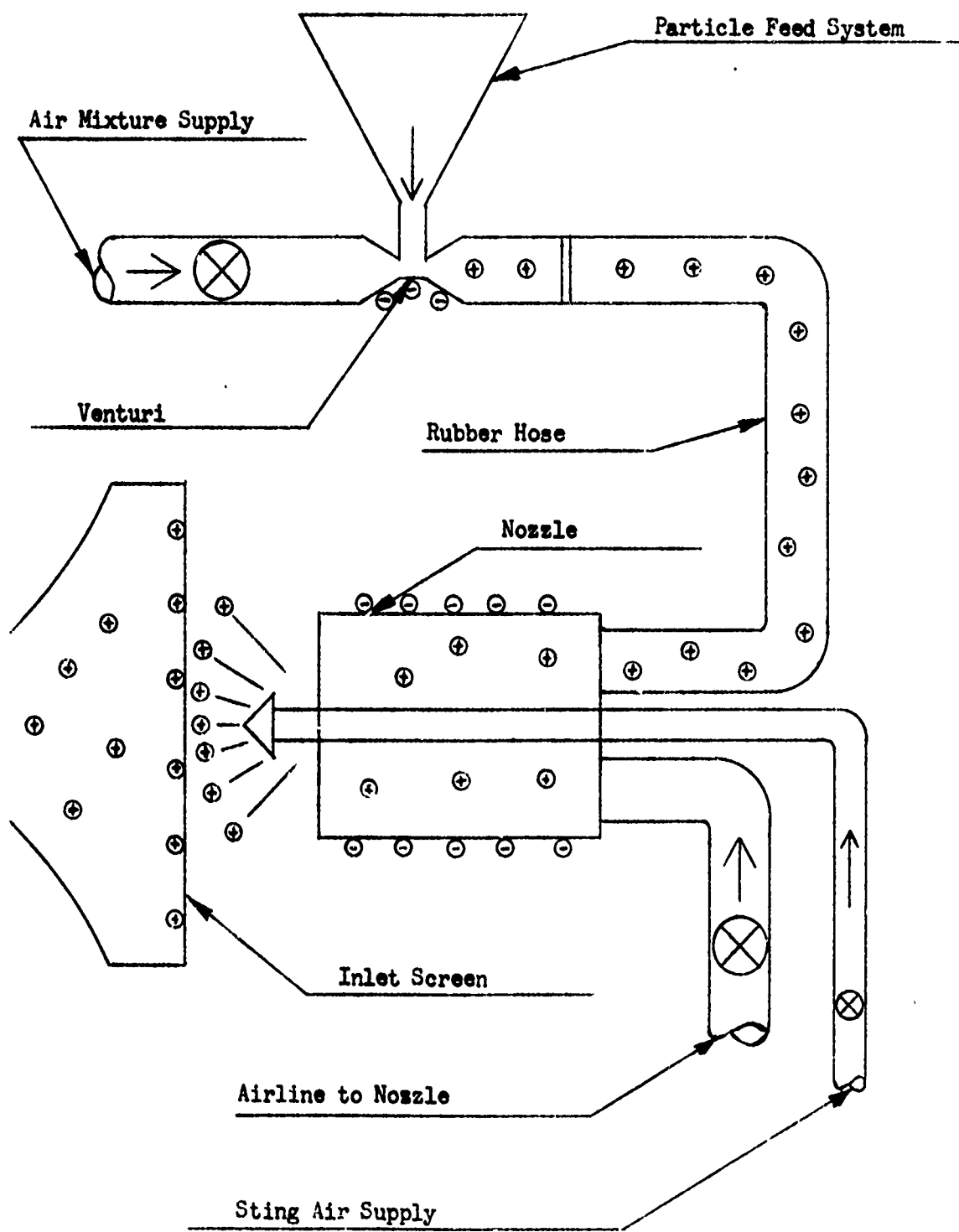


Table V

Air Supply Setting

Airline to Nozzle Turns Open	$\Delta P = 4''\text{H}_2\text{O}$ Nozzle Charge (μA)	Inlet Screen Charge (μA)
0	+0.65	+0.32
$\frac{1}{2}$	+0.35	+1.00
1	-0.6	+1.75
$1\frac{1}{2}$	-0.8	+2.00
2	-0.8	+2.2
$2\frac{1}{2}$	-0.8	+2.2

Table VI

Tunnel Speed vs. Charge at Inlet Screen

ΔP (inches H_2O)	Inlet Screen Charge (μA) (Airline to Nozzle Open One Turn)
4	+1.7
1	+1.4

4.4.1 PART I - Electrical Current Measurements for the Copper Cylinder Using the Wood Airfoil

The following series of tests were conducted to measure the electrical charging rate on the copper cylinder from the seeded air flow in the wind tunnel. The copper cylinder was located six feet downstream from the quarter chord position of the differential airfoil, except for Test 3. The wind tunnel speed was varied from a pressure drop of four inches of water to one inch of water.

1. The metal cylinder was traversed vertically in the wind tunnel with the differential airfoil removed. These tests were run to give an indication of the distribution of particles at various locations in the wind tunnel.

2. Tests similar to 1. above were conducted with the differential airfoil positioned at $\pm 0^\circ$, $\pm 7^\circ$, and $\pm 12^\circ$. These were the angles of attack Daugherty (2) used in his research.

3. Tests were run with the copper cylinder located at two and four feet downstream from the airfoils at the centerline position of the vortex for comparison to the tests in 2. above.

4. The frequency of oscillations at particular current levels was measured for the unfiltered current response at the centerline position of the vortex.

4.4.2 PART II - "Wetted Airfoil Phenomenon" Tests

This series of tests were used to investigate the "wetted airfoil phenomenon" and airfoil surface effects. The electrical charging

rate on the copper cylinder was measured. As in PART I, the copper cylinder was located six feet downstream from the quarter chord position of the differential airfoils, and the wind tunnel speed was varied from a pressure drop of four to one inch of water. The copper cylinder was located at the centerline position of the vortex.

5. A cloth wetted with tap water was placed over various surfaces of the airfoils. One test involved wetting both airfoils completely. In another test the inside surfaces of the crossed airfoils were wetted and in the final test the outside surfaces of the airfoils were wetted. See Figure 6 in Section 4.5.

6. Aluminum foil was used to cover the airfoil surfaces.

7. Oil was spread over the surface of the aluminum foil covered airfoils.

8. Oil was spread over the surface of the wood airfoil.

4.4.3 Procedure for Measuring Charging Currents

The following procedure was used for measuring the charging currents off of the copper cylinder.

1. Warm up time was required to stabilize the instruments from drifting too much.

2. The meter on the Keithley amplifier was zeroed and the output signal of the Keithley was zeroed and balanced with the oscilloscope.

3. The output gain was adjusted on the Keithley to 80 volts output for a full scale reading of $.4 \mu\text{A}$ current.

4. The sensitivity of the Brush strip chart recorder was adjusted to give full scale reading at $0.4 \mu\text{A}$ current.

5. The metal cylinder was polished with emery cloth and steel wool to give a shiny appearance.

6. The metal cylinder was placed in its test location of the wind tunnel.

7. The wind tunnel was started, and the air supply to the particulate feed system was turned on.

8. The wind tunnel speed was adjusted by the hinged doors to give a pressure drop of 4 inches of water.

9. The Keithley output was turned on and the Brush Recorder was turned on to record the current reading for approximately 10 seconds and then turned off.

10. The wind tunnel speed was adjusted in increments of one inch of water pressure drop, and the current output was recorded at each pressure increment.

11. The particulate feed system air line was turned off.

12. Finally, the wind tunnel motor was turned off.

Note: Ear protectors were worn while the wind tunnel and particulate feed system were in operation because of the high noise level existing.

4.4.4 PART III - Electrical Field Mill Tests

The following tests were conducted to measure the electrical field in the wood test cylinder. The test cylinder was located six

feet downstream from the quarter chord position of the differential airfoils. The wind tunnel speed was varied from a pressure drop of four to one inch of water.

9. The electrical field mill was traversed vertically in the seeded vortex flow with the wooden cylinder removed.

10. The electric field mill was placed in the wood cylinder to measure the electric field in the wood cylinder. The test cylinder, with the field mill in place, was traversed vertically in the seeded vortex flow.

4.5 Data from Experimental Results

The following results in this section will be given in the testing order described in Section 4.4.

As stated earlier in the chapter, the wind tunnel speed will be referred to as a pressure drop in inches of water. Table VII gives the pressure drop in terms of velocity, feet per second.

Table VII

Wind Tunnel Speed

Δp , Inches H_2O	Velocity ft./sec.
0	0
1	66
2	96
3	117
4	136

Abbreviations will be used to describe the location of the test body in the wind tunnel test section. These abbreviations are given in Table VIII.

Table VIII

Location of Test Body

Abbreviation	Location
3 DU	Three diameters of the test body above centerline.
CL	Centerline.
3 DD	Three diameters below centerline.

Note: One diameter of the test body equals 2 inches.

In studying the "wetted airfoil phenomenon," various surfaces of the differential airfoil were covered with a wetted cloth. Figure 6 shows the surfaces described and gives the abbreviations used in Figure 22.

Figure 6

Differential Airfoils

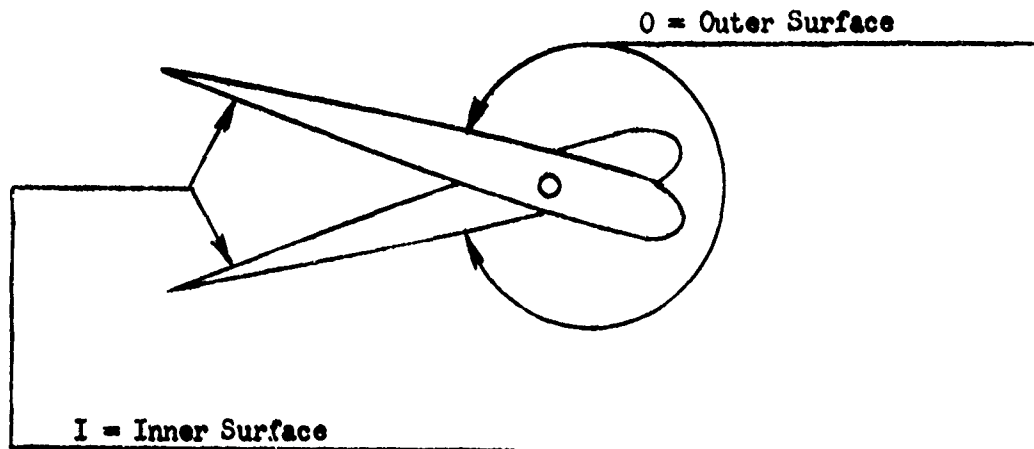


Figure 7

**No Airfoil, Location
Copper Cylinder**

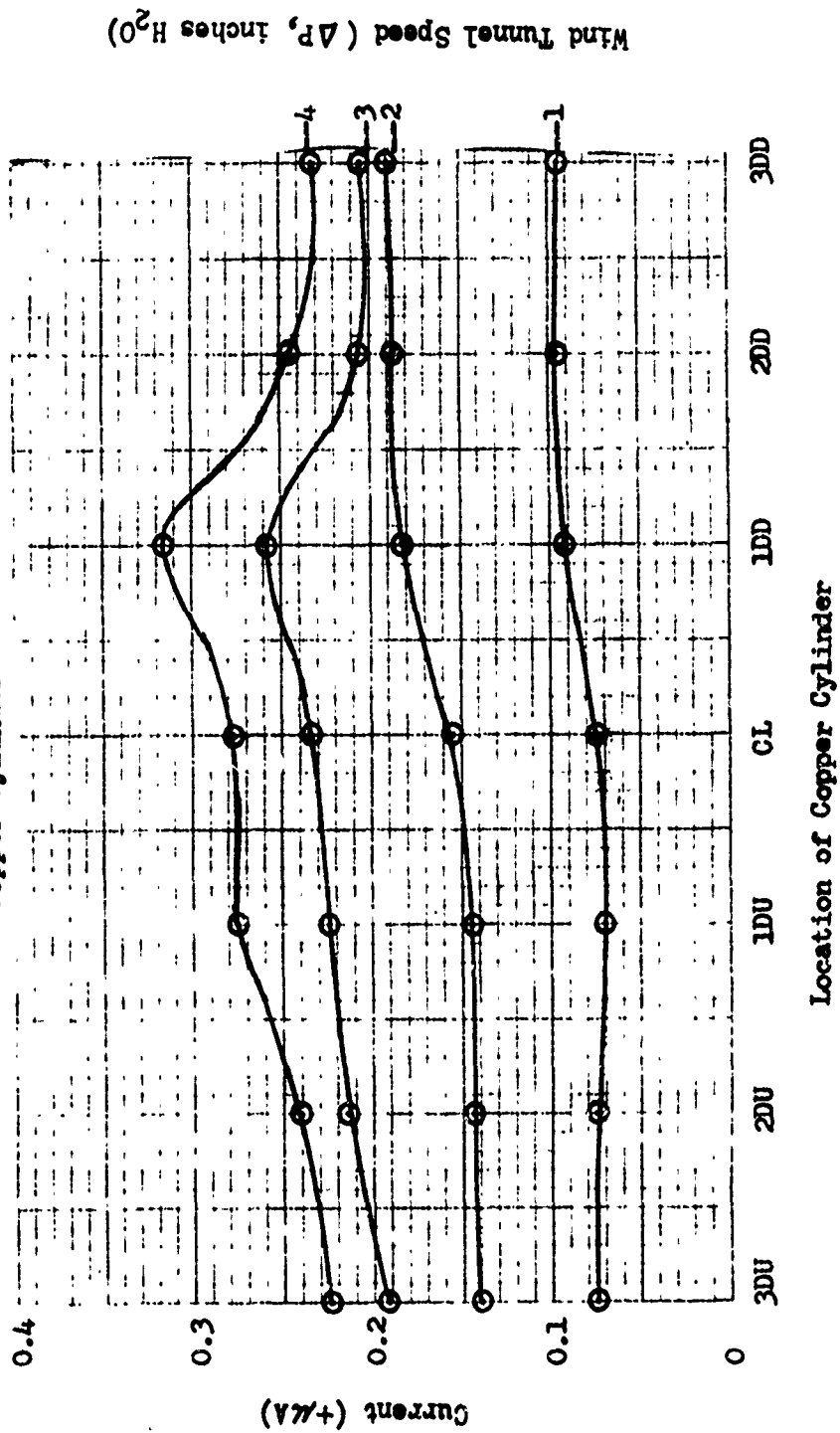


Figure 8

No Airfoil, Centerline
Copper Cylinder

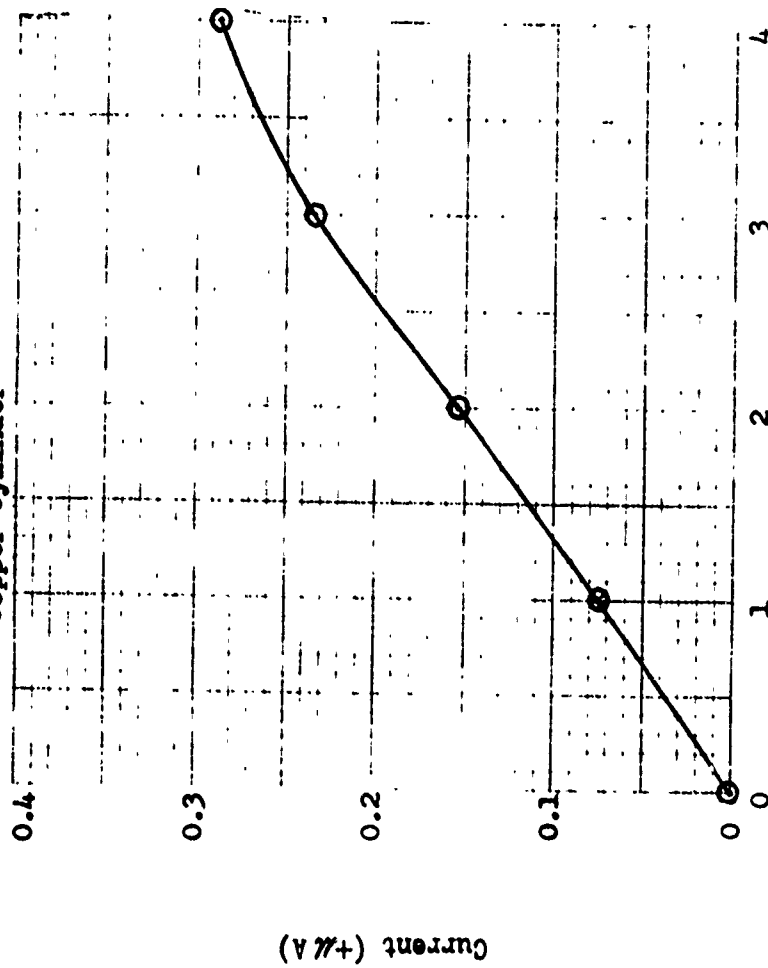


Figure 9
 $\pm 0^\circ$ Wood Airfoil, Location
 Copper Cylinder

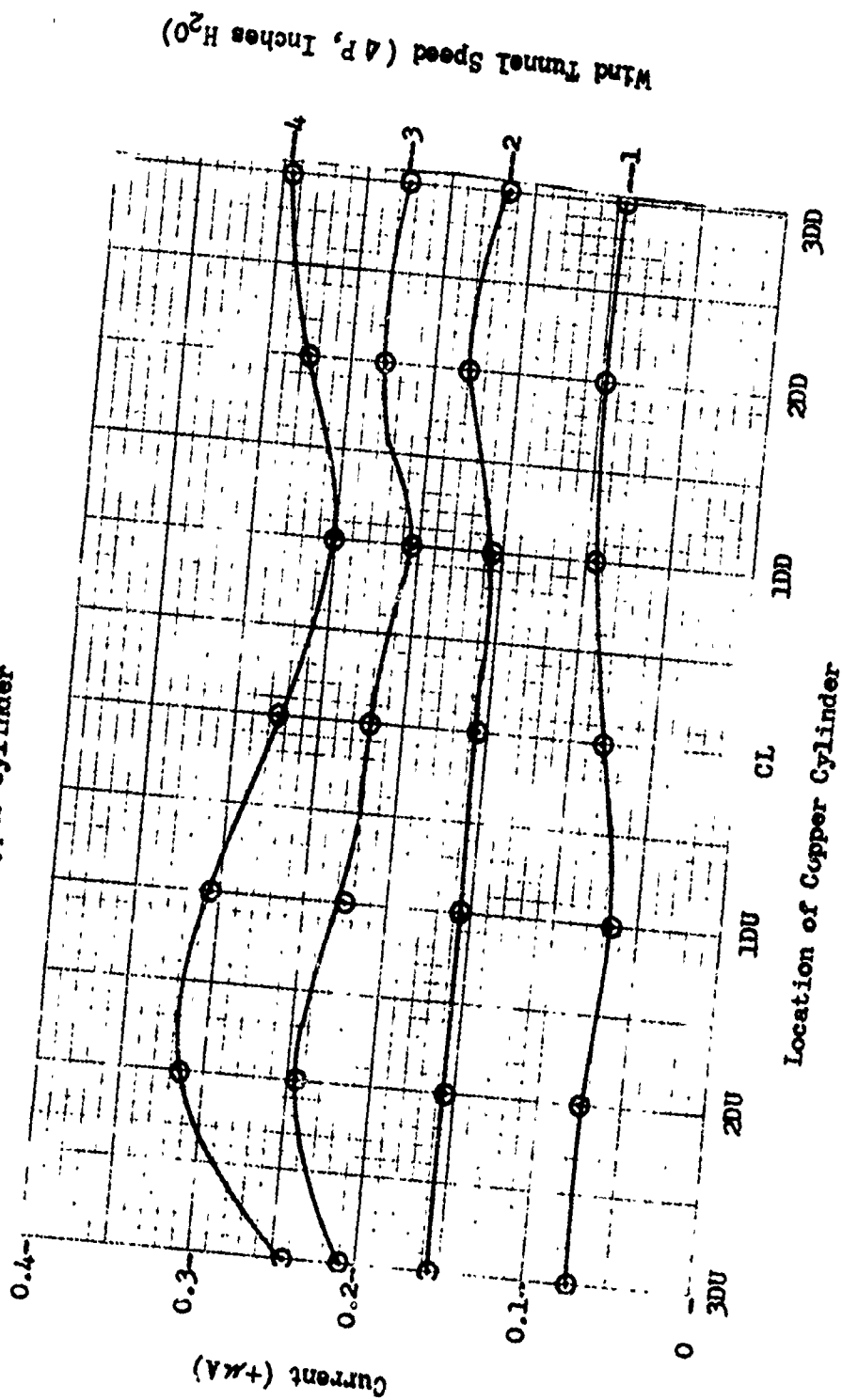
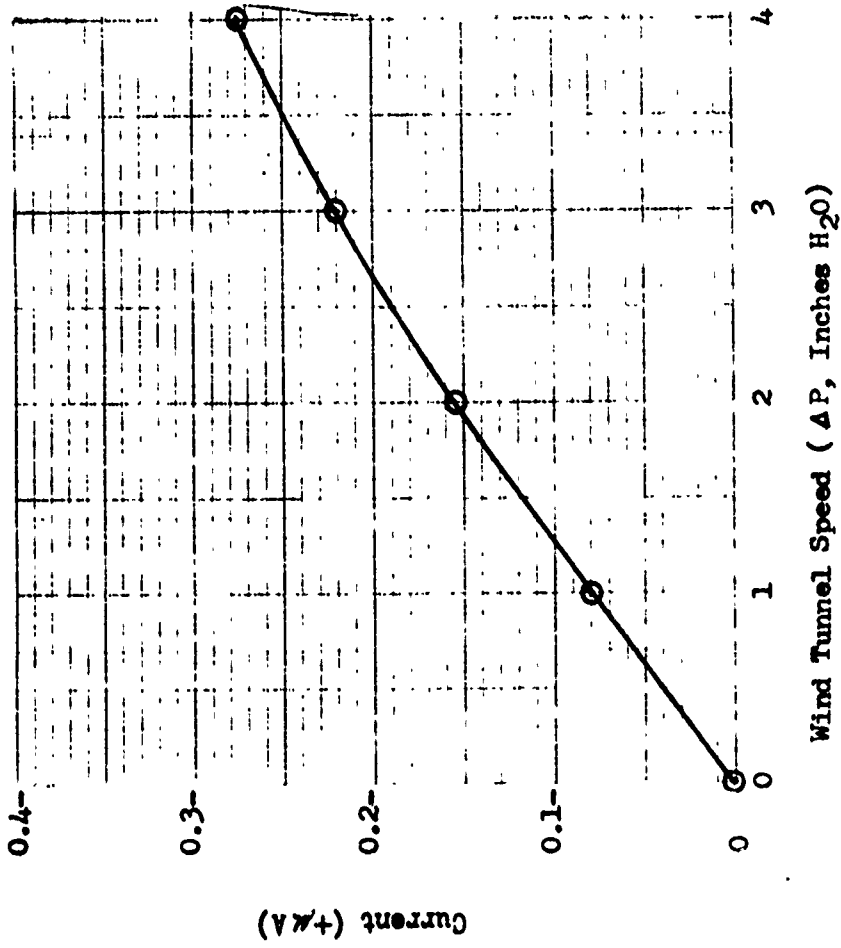


Figure 10

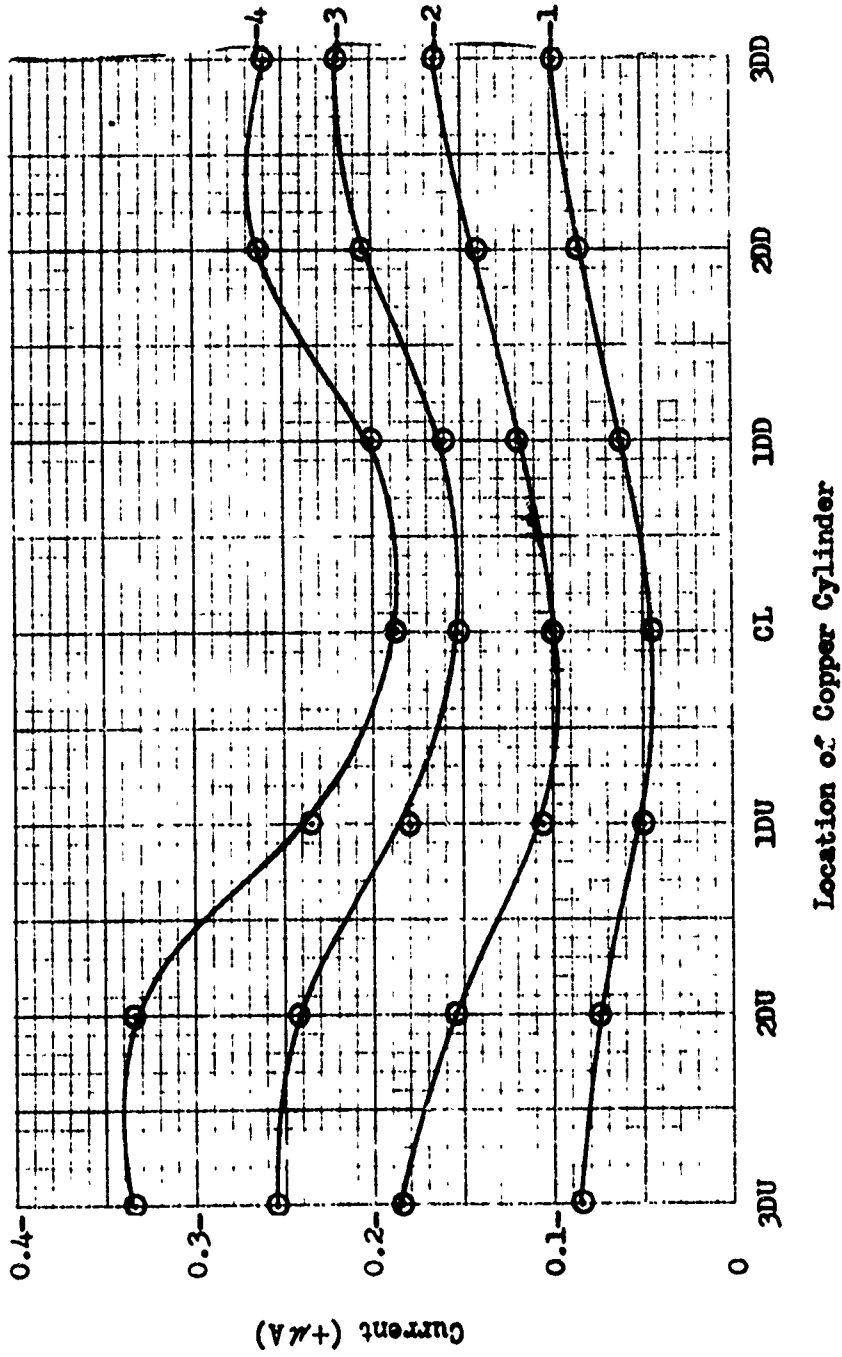
$\pm 0^\circ$ Wood Airfoil, Centerline
Copper Cylinder



Reproduced from
best available copy.

Figure 11

$\pm 7^\circ$ Wood Airfoil, Location
Copper Cylinder



Wind Tunnel Speed (ΔP , Inches H_2O)

Figure 12

$\pm 7^\circ$ Wood Airfoil, Centerline
Copper Cylinder

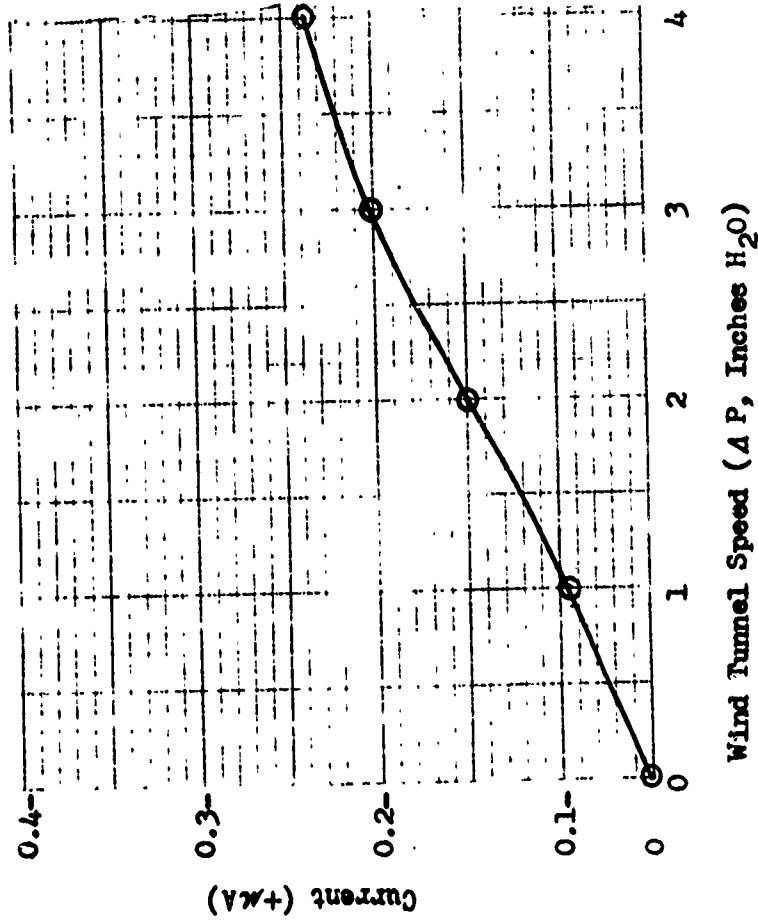
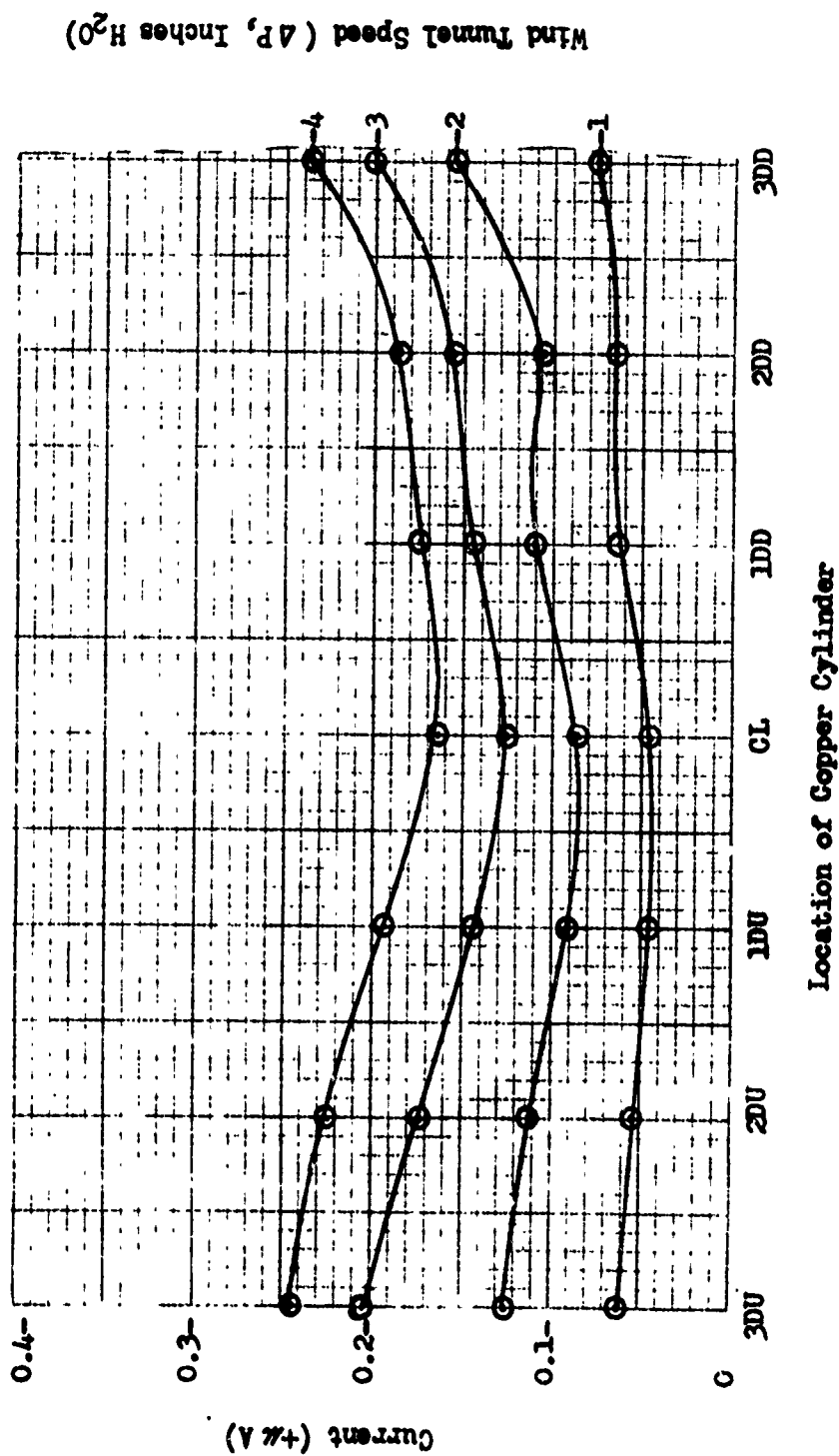


Figure 13

**+ 12° Wood Airfoil, Location
Copper Cylinder**



Reproduced from
best available copy.

Figure 1A

+ 12° Wood Airfoil, Centerline
Copper Cylinder

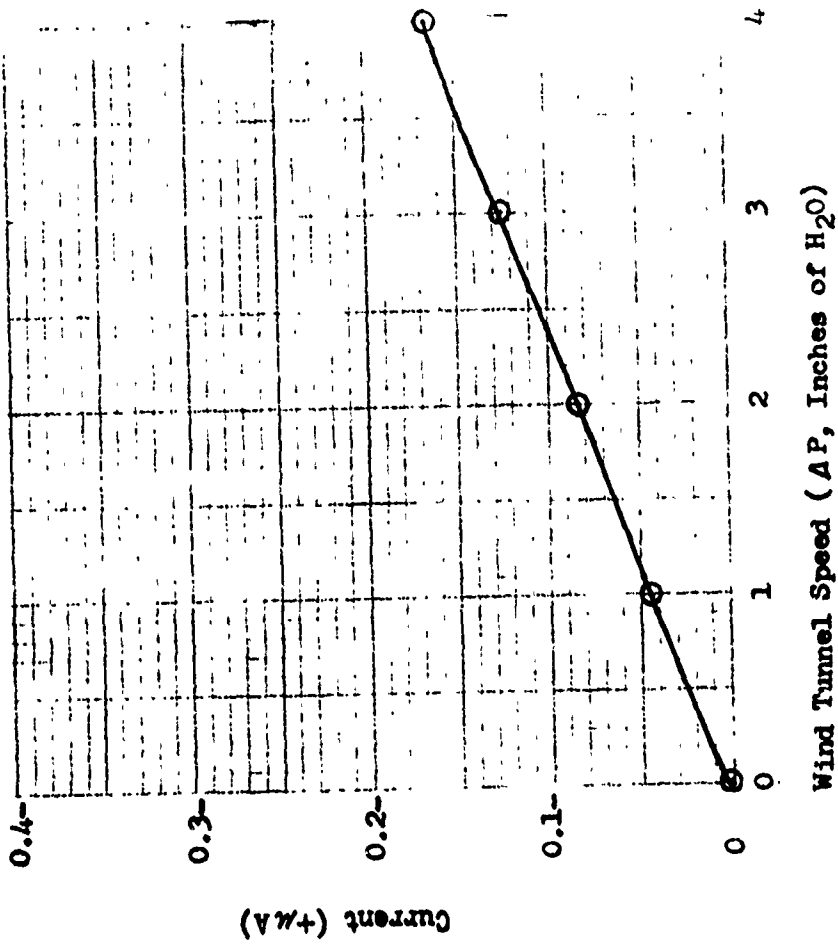


Figure 15

Centerline Charging Rates
Compared for Angles of Attack
for Wood Airfoil
Copper Cylinder

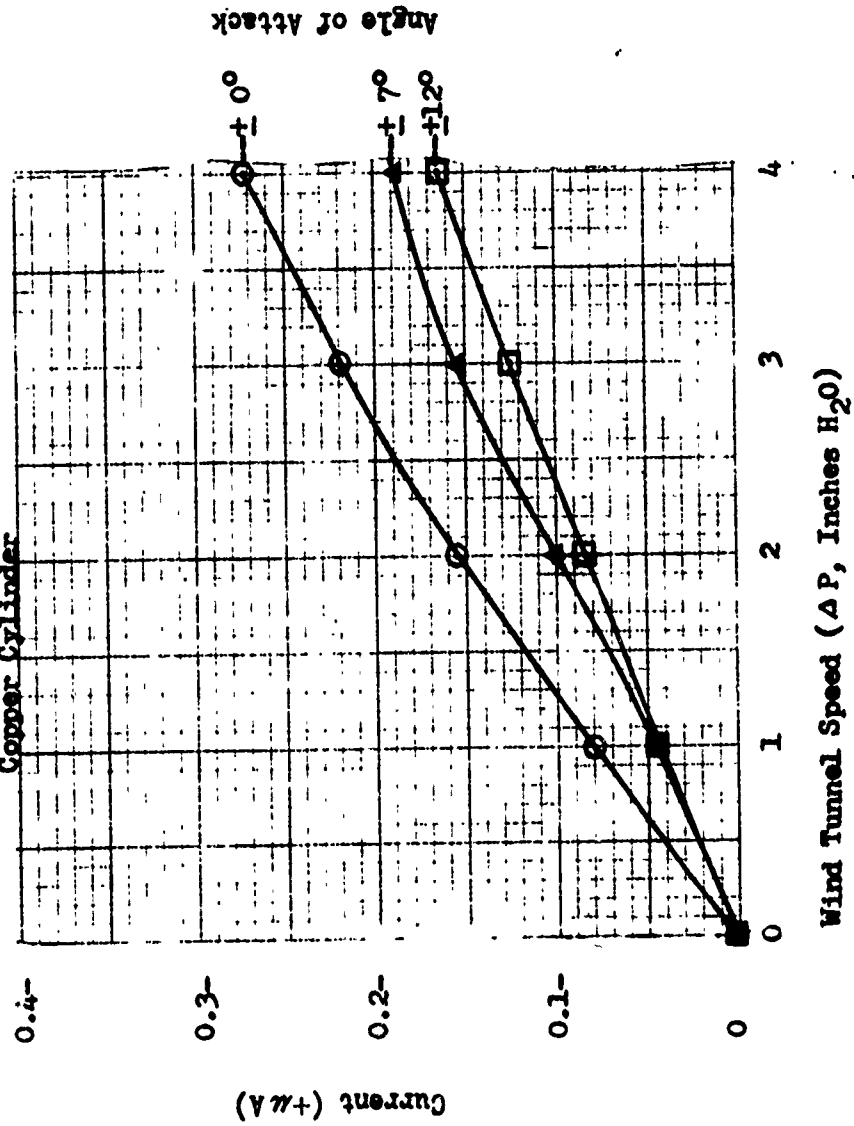
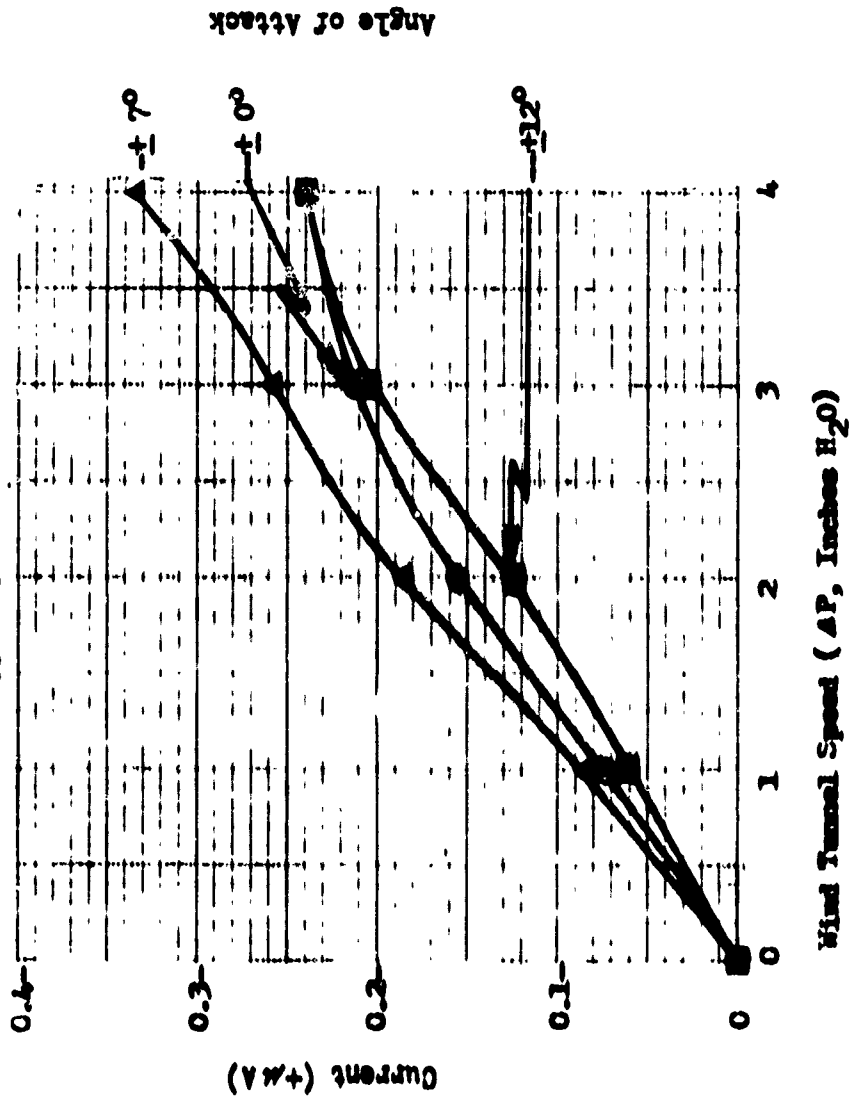


Figure 16

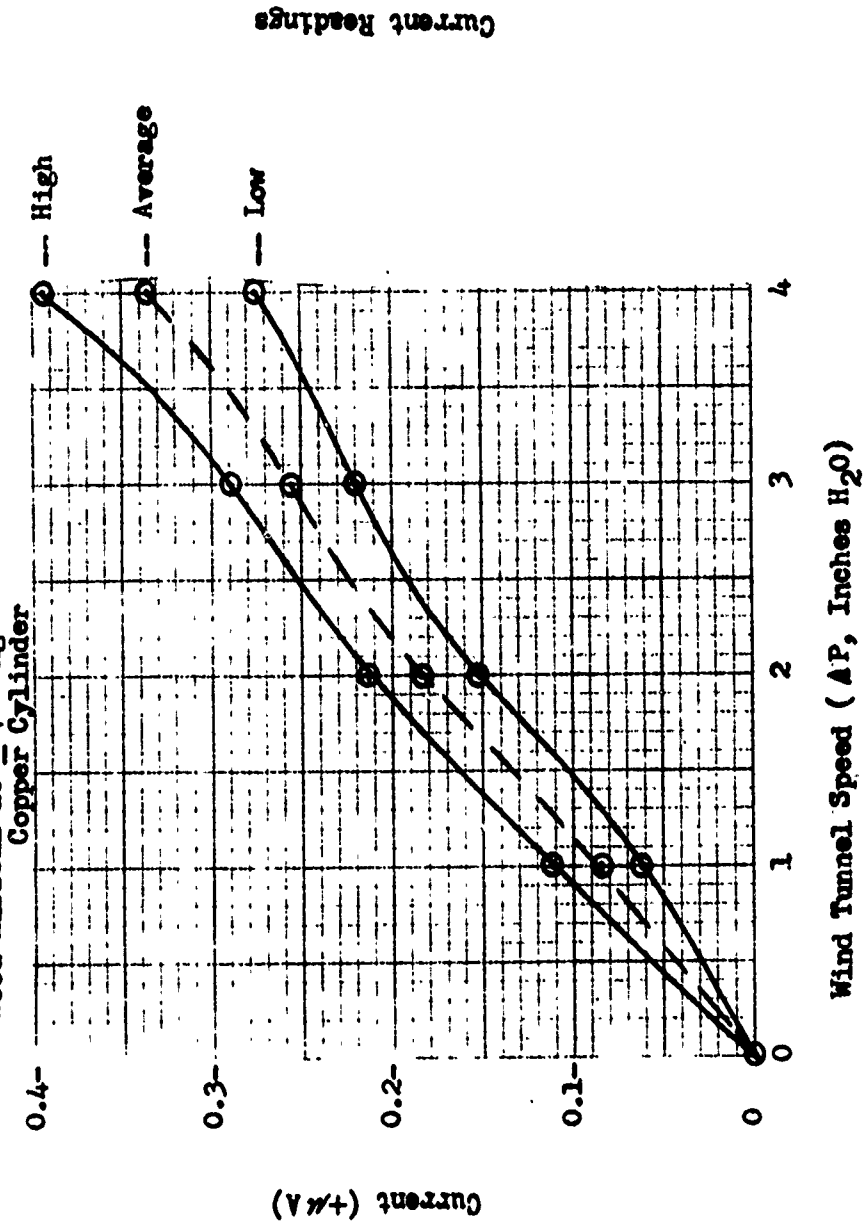
3 Diameters Above Centerline (300)
Angles of Attack Compared
for Wood Airfoil
Copper Cylinder



Reproduced from
best available copy.

Figure 17

Typical Charging Range
3 Diameters Above Centerline (3DU)
Wood Airfoil at +7° Angle of Attack
Copper Cylinder



Current Readings

Figure 18

Brush Recorder Output
Indication of Range of Charge
3 Diameters Above Centerline, $\pm 7^\circ$ Angle of Attack
Wood Airfoil, Copper Cylinder
Paper Rate: 5 mm./sec.

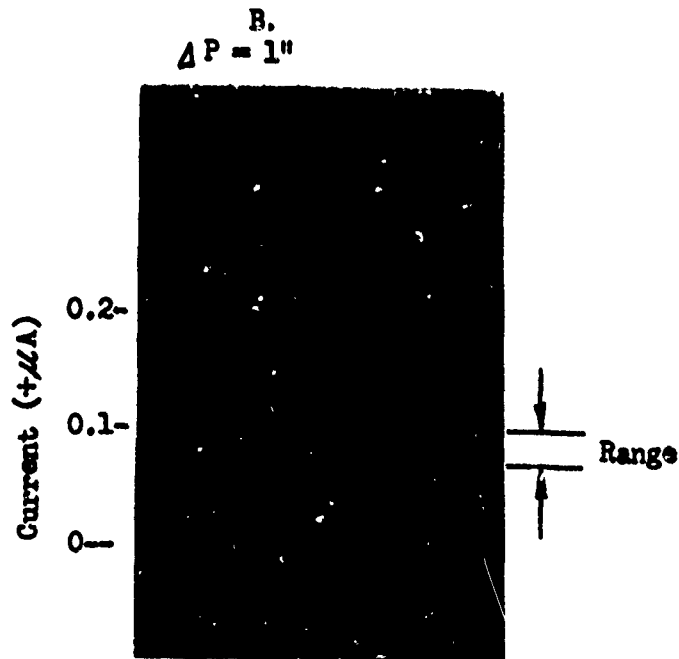
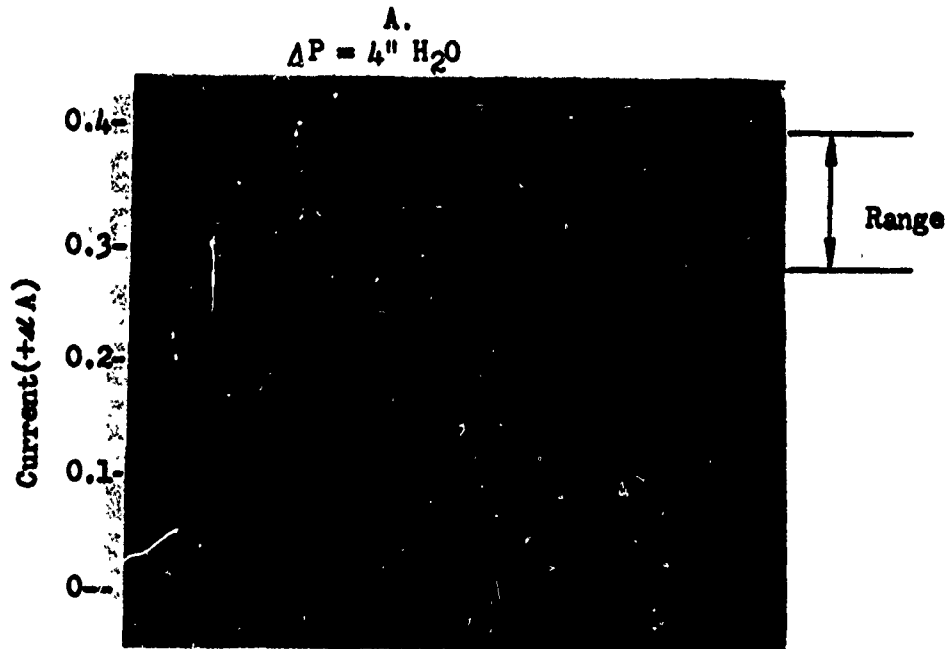


Figure 19

Distance from Airfoil
Centerline, + 7° Angle of Attack
Wood Airfoil, Copper Cylinder

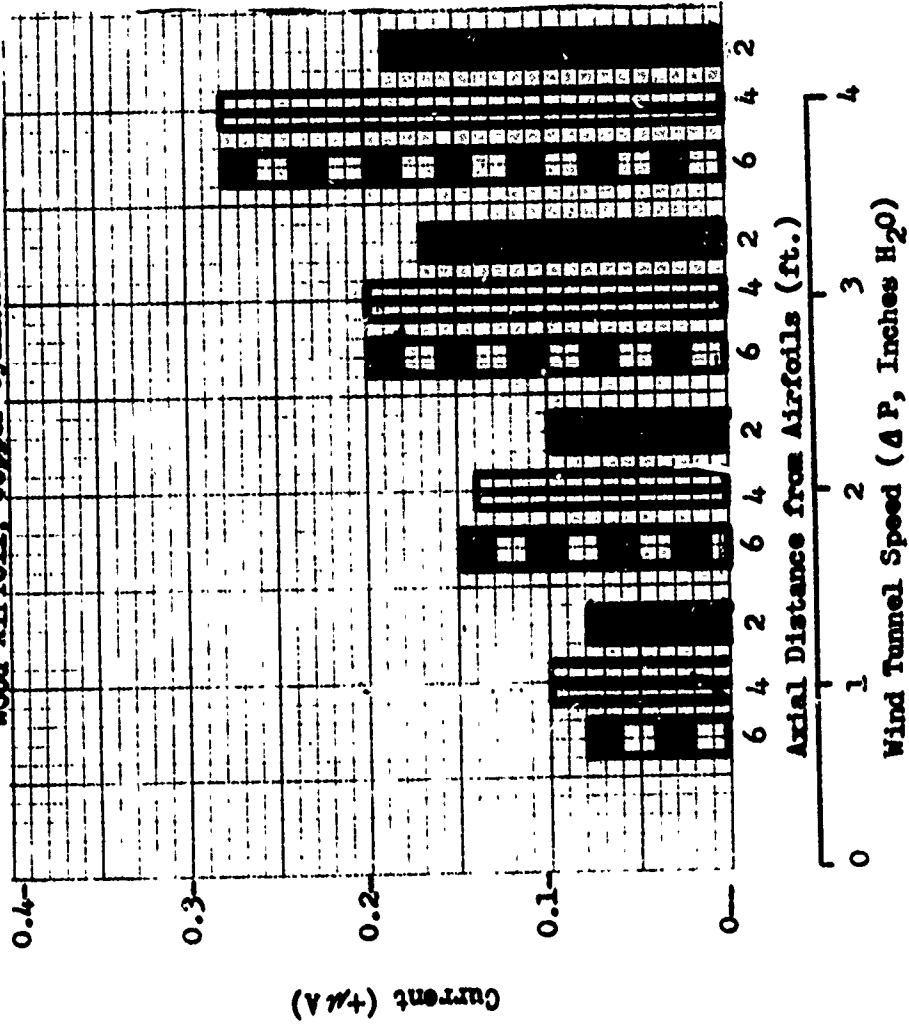


Figure 20

Frequency of Counts at Current Levels
Centerline, $\pm 7^\circ$ Angle of Attack, $\Delta P = 4'' \text{ H}_2\text{O}$
Wood Airfoil, Copper Cylinder
No Filter

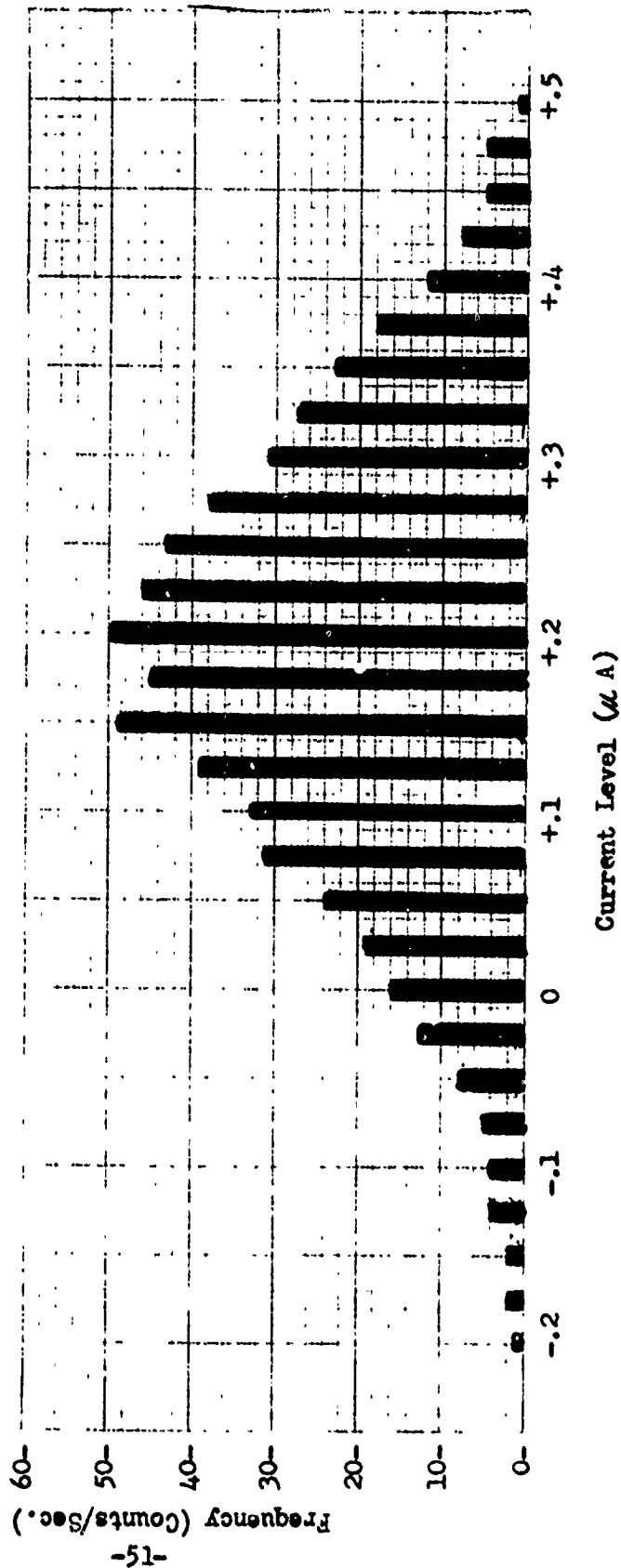


Figure 21

Probability Plot for Frequency of Counts
Centerline, $\pm 7^\circ$ Angle of Attack, $\Delta P = 4'' \text{ H}_2\text{O}$
Wood Airfoil, Copper Cylinder

50 Counts = 100%

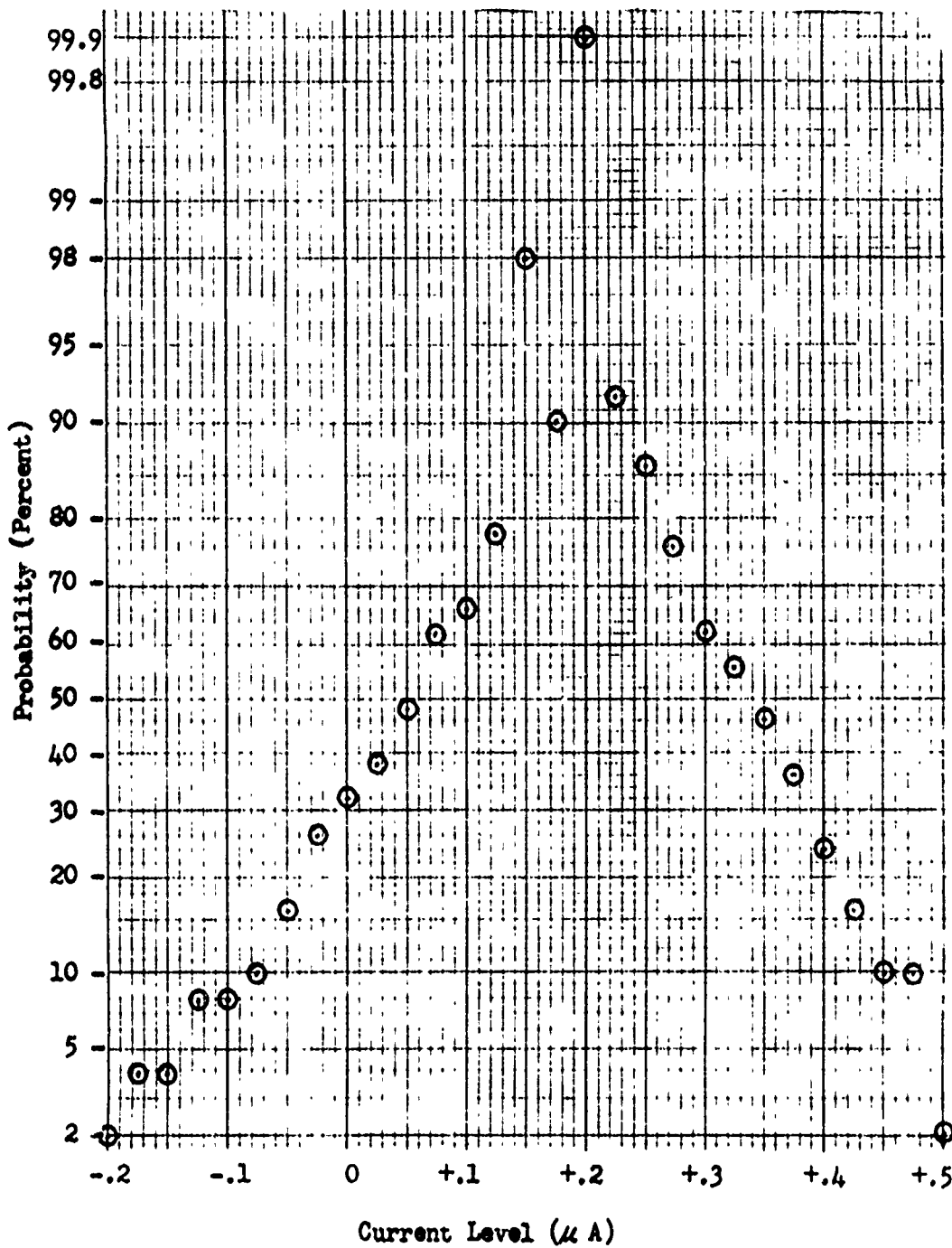


Figure 22

Wetted Wood Airfoil
Centerline, $\Delta P = 4'' \text{ H}_2\text{O}$
Copper Cylinder
(Note: See Figure 6 for Notation)

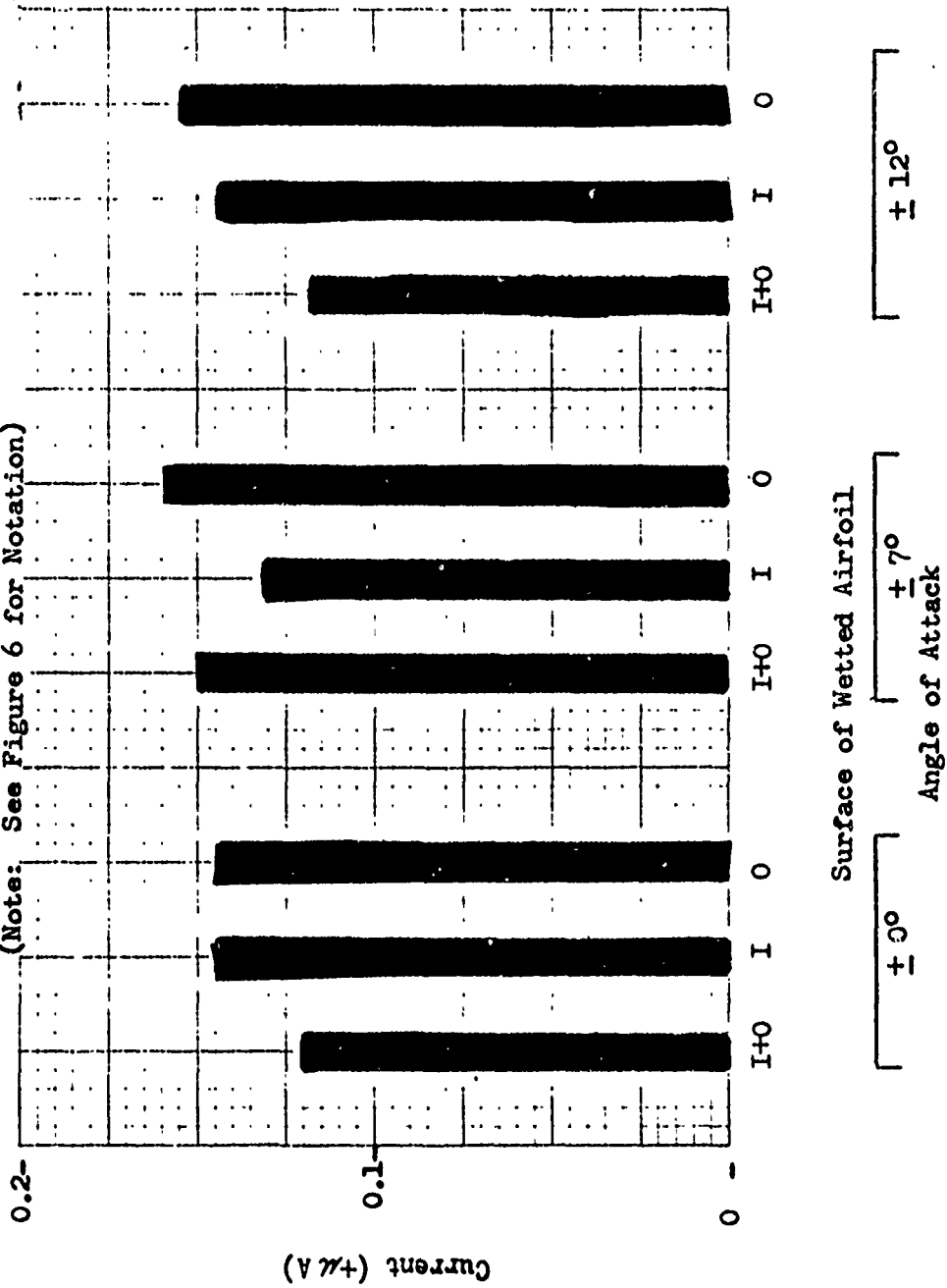


Figure 23

Charging Rates with Aluminum Foil Airfoil
For Copper Cylinder and Aluminum Foil Airfoil
Centerline, $\pm 0^\circ$ Angle of Attack

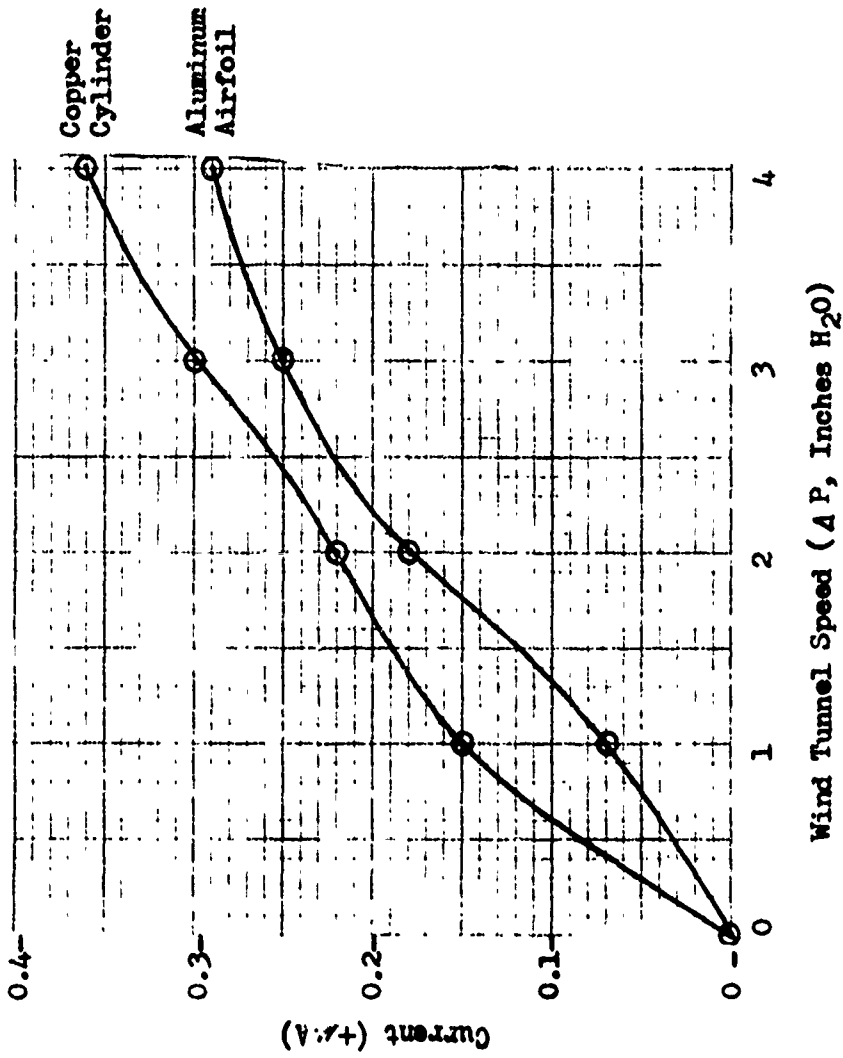


Figure 24

Charging Rates with Aluminum Foil Airfoil
For Copper Cylinder and Aluminum Foil Airfoil
Centerline, $\pm 7^\circ$ Angle of Attack

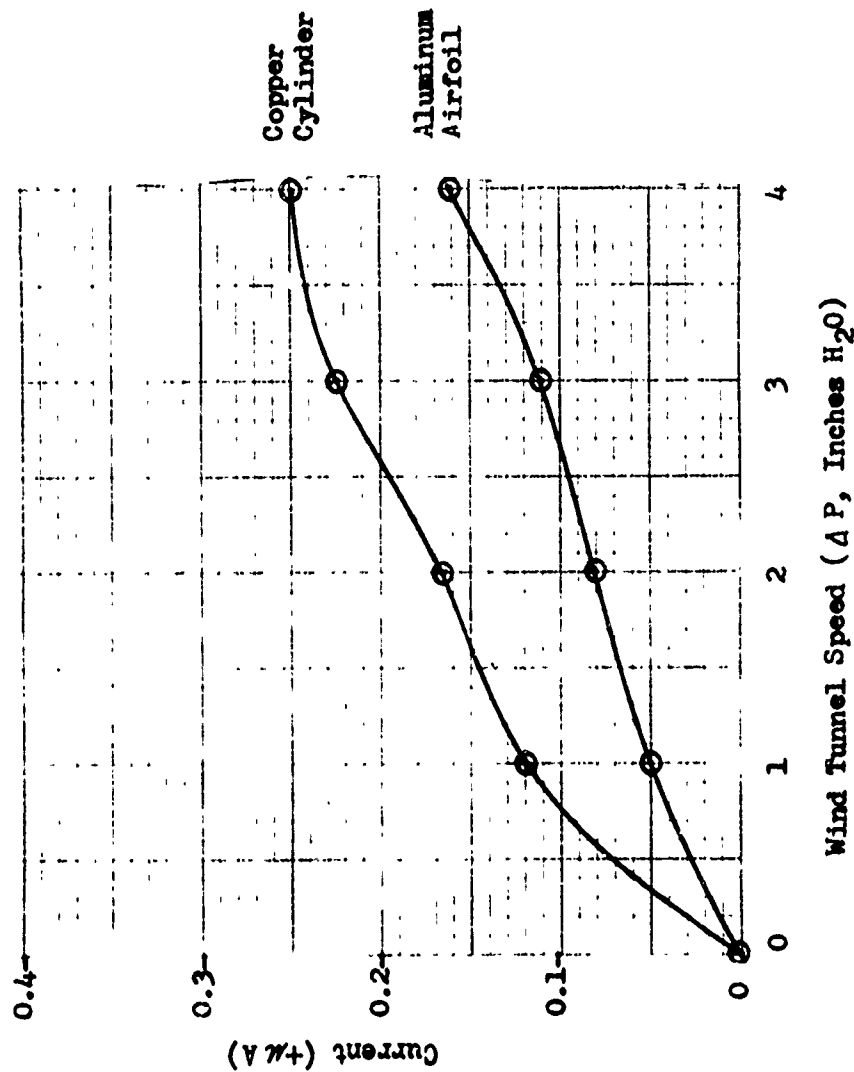
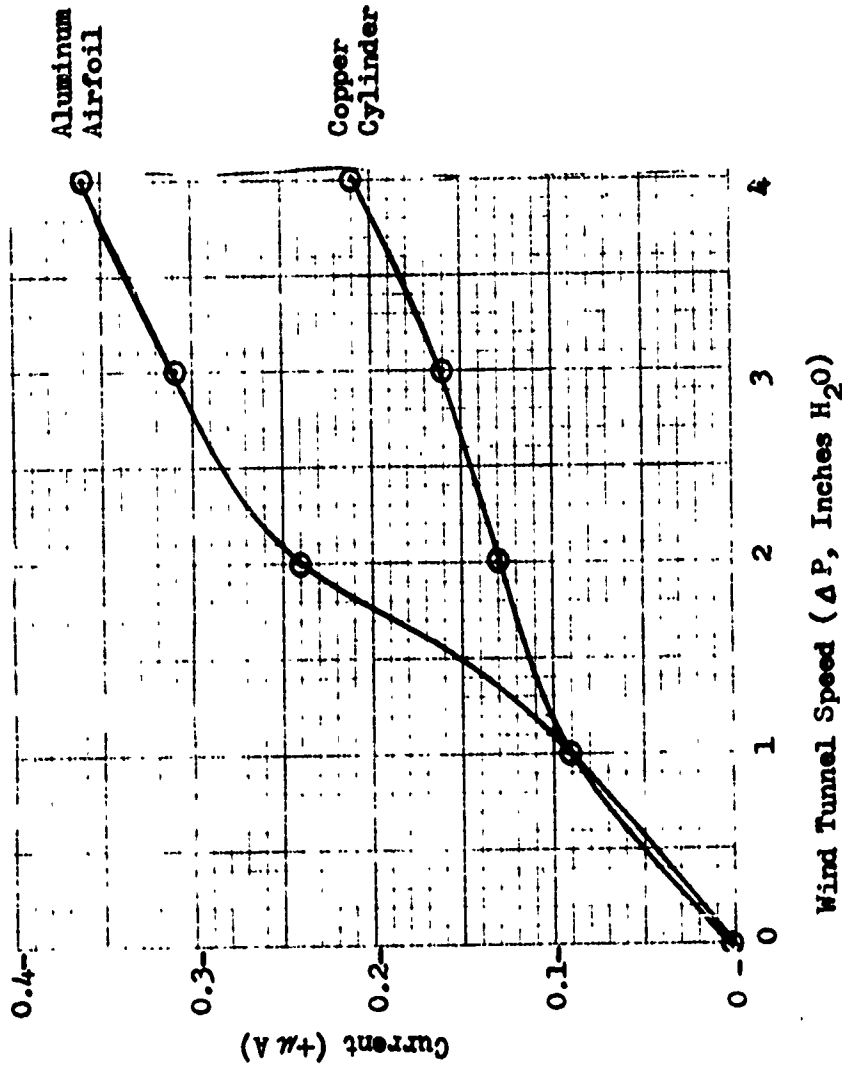


Figure 25

**Charging Rates with Aluminum Foil Airfoil.
For Copper Cylinder and Aluminum Foil Airfoil
Centerlines, $\pm 12^\circ$ Angle of Attack**



Reproduced from
best available copy.

Figure 26

Charging Rates with Oil on Aluminum Foil Airfoil
For Copper Cylinder and Aluminum Foil Airfoil
Centerline, $\pm 7^\circ$ Angle of Attack

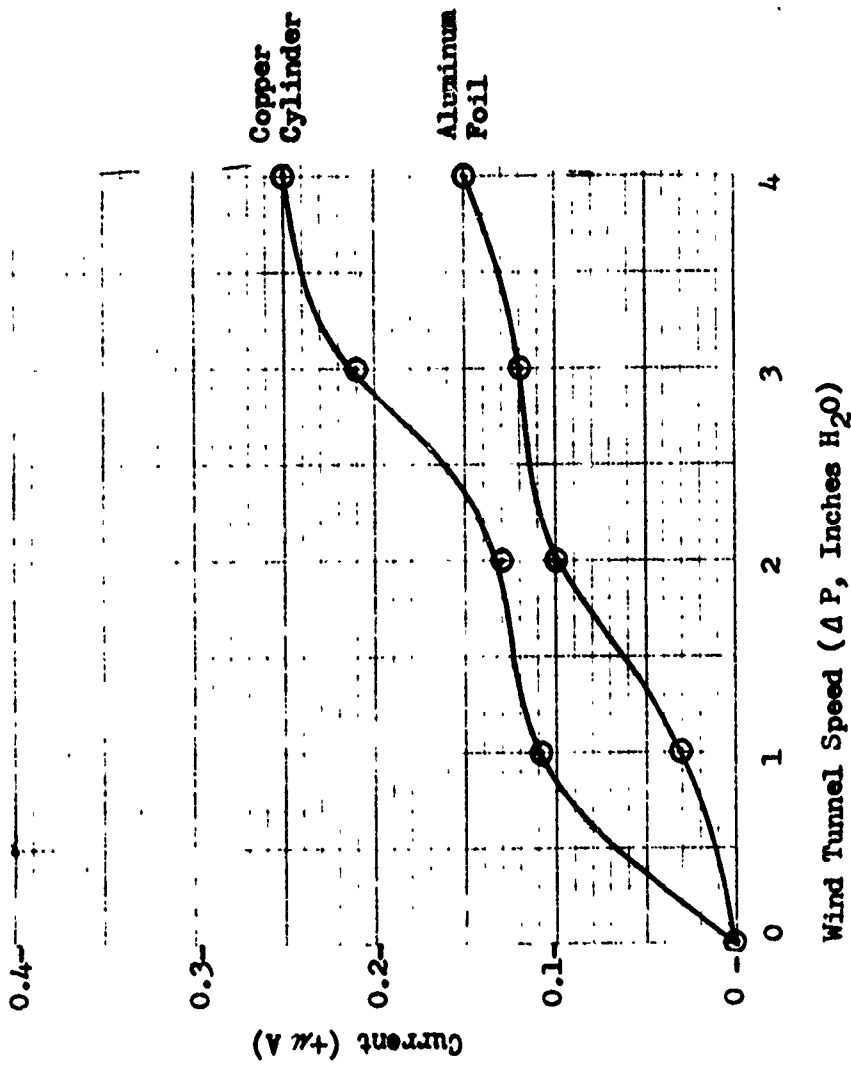


Figure 27

Typical Field Mill Traces
Oscilloscope: 1 mV/cm., 5 m.sec/cm.

^A
Field Mill Alone
Centerline, $\pm 7^\circ$ Angle of Attack, $\Delta P = 4'' \text{ H}_2\text{O}$



^B
Field Mill in Wood Cylinder
Centerline, $\pm 0^\circ$ Angle of Attack, $\Delta P = 4'' \text{ H}_2\text{O}$



Figure 28

Electrical Field Mill Output, Location
 ± 70 Angle of Attack, $\Delta P = 4 \text{ } ^\circ\text{H}_2\text{O}$, Wood Airfoil

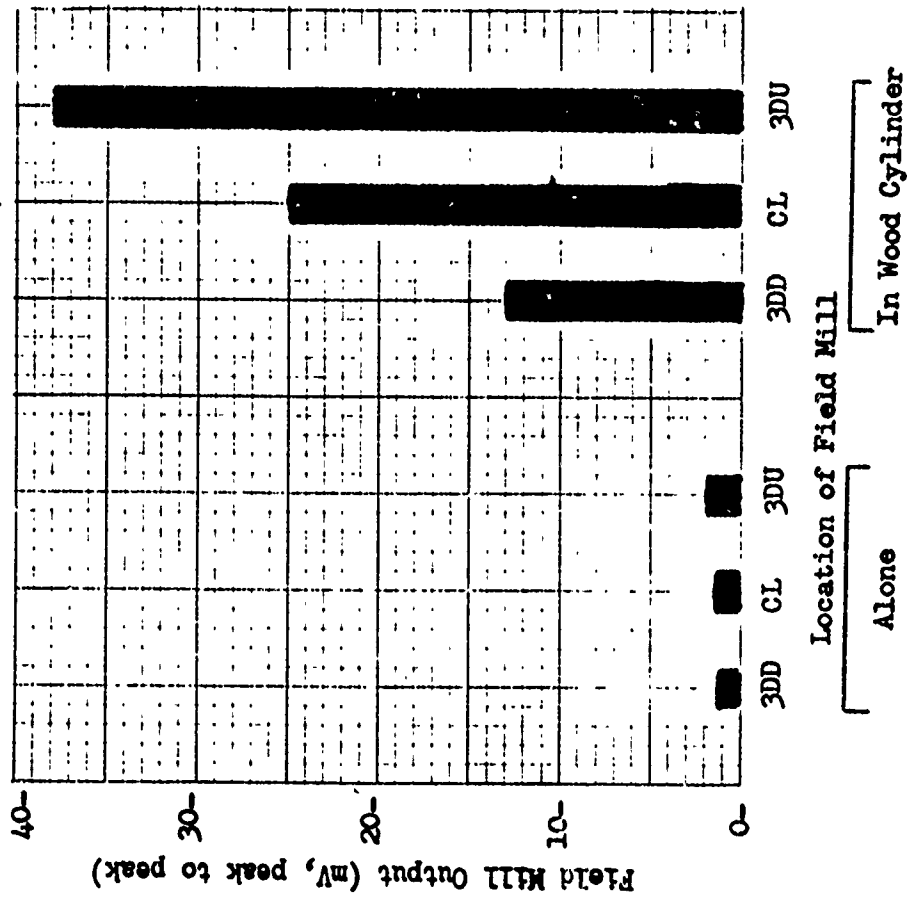
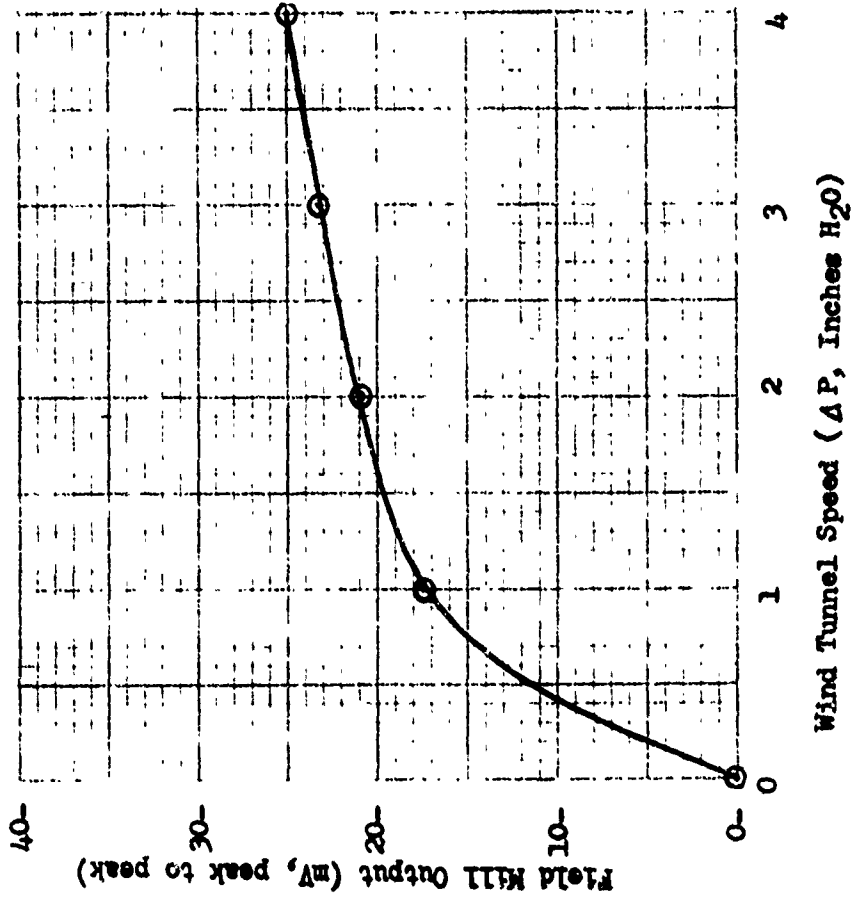


Figure 29

Electrical Field Mill Output in Wood Cylinder
 $\pm 7^\circ$ Angle of Attack, Centerline, Wood Airfoil



Reproduced from
best available copy.

V. DISCUSSION OF RESULTS

The test conducted to measure the charging rate with no airfoil, indicated a maximum current at one diameter below centerline, Figure 7. It was also found that the current was less at the wall boundaries because of reduced velocity at these boundaries, therefore, leaving the entrained charged particles in the central region of the test section. Although the maximum charging rate was not always at the centerline position, the measured currents were fairly constant with respect to location of the test body, thus indicating a uniform spread of charged particles throughout the test section. At lower wind tunnel speeds, higher current readings were found for the locations below centerline. This may be explained by the fact that the reduced velocity did not entrain as many particles, therefore leaving a higher concentration of particles near the lower surface because of the force of gravity on the particles.

The charging rate increased almost linearly with the wind tunnel pressure drop for various airfoil angles of attack as shown by Figures 8, 10, 12, 14. This fact may be explained by referring to the Section 4.3 on charge generation. At higher velocities, the PVC particles had more frictional contact with the inlet screen and the metal inlet housing, thus giving the PVC a higher electrical charge. At reduced wind tunnel velocities, the charging rate decreased, possibly because of the reduced frictional contact needed for charge generation.

With the wood airfoil placed at angles of attack of $\pm 7^\circ$ and $\pm 12^\circ$, a definite lowering of the charging rate occurred at the centerline position for various wind tunnel speeds, Figures 11, 13. The magnitudes of the measured current were similar for $\pm 0^\circ$ and $\pm 7^\circ$ angles of attack; although, the maximum current reading for the $\pm 12^\circ$ angle of attack was substantially reduced from the other angles of attack. Possibly, the vortex produced by the $\pm 12^\circ$ angle of attack caused the PVC particles to be thrown out farther from the center of the vortex, thus giving an indication of a reduced charging rate at the tested locations. Figure 15 compares charging rates at the centerline for various angles of attack. As the angle of attack was increased, the charging rate was reduced. The increased angle of attack, as suggested earlier, does throw out the PVC particles farther from the center of the vortex, as was visually verified by observing a white ring of PVC at the test location. Comparison of charging rates at three diameters above the centerline, does indicate increased charging for the $\pm 7^\circ$ angle of attack, while the charging rate for the $\pm 0^\circ$ and $\pm 12^\circ$ angles of attack were approximately equal, Figure 16. One may expect the $\pm 12^\circ$ angle of attack to show a higher current reading than the $\pm 7^\circ$ angle of attack because the PVC would be thrown out farther from the center of the vortex. Possibly the PVC was thrown out farther than the test location of three diameters above or below centerline, and therefore, the maximum current was not measured.

At low wind tunnel speeds the curves in Figures 7, 9, 11, and 13 flatten out quite a bit. This shows an almost constant current reading for various test locations. This may indicate a relaxed effect of the airfoil on creating a vortex capable of distributing the PVC to its outer region for low air speed operation.

All of the data previously discussed was plotted by taking the average between the highest and lowest current readings from the Brush Recorder for a particular test. Figure 17 shows a plot of the high, low, and average currents for a typical test. These fluctuations in current readings were reduced somewhat at lower wind tunnel speeds. Figures 18A and B show the Brush Recorder output for relatively fast and slow wind tunnel speeds. The range in current readings is substantially reduced at lower wind tunnel speeds.

Since all tests were conducted at a location six feet downstream from the differential airfoils, a sample test was conducted at two feet and four feet downstream from the airfoil for comparison purposes, Figure 19. This test was not altogether conclusive, although it did indicate less charging at two feet than either four or six feet. Possibly at such a relatively close location to the airfoils, the vortex was not fully established and the airfoils forced the flow system away from the test body in a manner such that it did not become charged adequately.

The Monsanto Counter was used to count the frequency of oscillations at various current levels for the unfiltered current

measurement. A histogram of counts per second for various current levels is plotted in Figure 20. The maximum number of counts occurred at a current reading of + 0.2 μ A, which was also the current measured with the filtered current response. The frequency of counts above or below the current reading with the maximum number of counts decreased in a symmetrical manner about the maximum current reading in the familiar "bell shaped" probability curve. Assuming the highest frequency of counts, fifty counts per second, as 100 percent, a probability plot was made for various current levels using the standard Gaussian distribution probability paper, Figure 21. This data plotted in a manner to give two almost straight line plots, which indicate normal distribution.

A cloth wetted with water was wrapped around the differential airfoils to study the "wetted airfoil phenomenon." Figure 22 shows the results of this testing for the various wetted surfaces. See Figure 6 for notation. A drastic reduction in charging rates was observed for the wetted surfaces compared to the dry airfoil tests. The lowest currents observed were for both the inner and outer surfaces wetted. More tests should be conducted in this area to get conclusive results, although these tests did indicate partially that the inner surface of the airfoils seemed to reduce the current more than the outer surface did. The reduced charging in this case may be attributed to the alteration of the contact charging mechanism brought about by the wetted airfoils. Also, it may be possible that the wetness of the airfoils helped to discharge the charged particles as they impacted the surface.

The next series of tests involved using a conducting airfoil; in this case the wood airfoils were wrapped tightly with aluminum foil. The results of these tests showed that the charging rate on the copper cylinder was increased somewhat by using the aluminum airfoil as compared to using the wood airfoil, possibly by more frictional charge build-up on the PVC from frictional contact with the aluminum foil differential airfoils. Figures 23, 24, and 25 show charging rates for the cylinder and airfoil, although no conclusive results were established relating the charging rates to each other.

Again to study the "wetted airfoil phenomenon," some 10 W - 40 motor oil was spread over the surface of the aluminum foil airfoils to determine its affect on the charging rates. No appreciable change was observed in charging rate for the cylinder testing and for the oiled and clean aluminum foil airfoils as one can clearly see by comparing Figures 24 and 26. Oil was also spread over the surface of the wood airfoil and the charging rate on the copper cylinder remained the same as the dry wood airfoil. The dielectric constant of the oil may have been very close in magnitude to the dielectric constant of the varnished airfoil and wind tunnel surfaces so that no appreciable change in current would result.

When the electrical field mill was placed in the seeded vortex flow alone, an electrical field was measured which "jumped" around quite a bit as can be seen in Figure 27A. These "jumps" occurred

as a result of the charged PVC particles striking the exposed stator of the field mill head. Figure 27B shows the field mill output with the field mill placed in the wooden cylinder. A plot of the field mill output at various test locations for the field mill alone and in the wooden cylinder is shown in Figure 28. The results of tests with the field mill alone indicated no general trend in the electrical field as it was traversed through the vortex, other than the fact that all the output traces were approximately equal, about 12,000 volts/meter. However, with the electrical field mill placed in the wooden cylinder, the electrical field increased drastically from the lower surface of the wind tunnel to the upper surface of the wind tunnel. Figure 28 shows the maximum output of the field mill to correspond to 250,000 volts per meter. A polarity check showed the electrical field to be positive in sign. This strange result was confirmed by several similar tests. The only explanation the author has to this strange result is the location of the test. A plexiglass door was located at the upper surface of the wind tunnel at the particular location, while the other surfaces of the tunnel at the location were wood coated with varnish. Possibly, the plexiglass door became more charged from the PVC than the varnished surfaces of the wind tunnel, thus indicating a large electric field near the plexiglass door. A plot of the electrical field mill output versus wind tunnel speed, shows an increase in electrical field with an increase in wind tunnel speed, Figure 29.

VI. CONCLUSIONS

This experimental study determined general charging trends for a cylindrical body placed in a vortex "seeded" with charged particulate. Several interesting facts were discovered about the charging phenomenon, the wetting of the differential airfoil, and electrical field produced. Although, no empirical relations were developed, general trends were found to exist.

The following is a summary list of conclusions:

1. The differential airfoil produced a stable vortex capable of distributing the charged PVC particles throughout the vortex.
2. As the angle of attack for the differential airfoils was increased, making a larger diameter vortex, the charged particles were thrown out farther from the center of the vortex. The charging rate on a cylindrical body placed at the center of the vortex was decreased.
3. The charging rate on the cylindrical body increased directly with the wind tunnel speed. This probably occurred as a result of frictional charging of the PVC as it came in contact with the inlet screen and metal inlet housing.
4. Fluctuations in charging were reduced with lower wind tunnel speeds.
5. A normal Gaussian distribution was found to exist for charging of the metal cylinder.

6. An airfoil wetted with water was found to reduce the charging rate on the metal cylinder.
7. The aluminum foil airfoil helped to increase the charging rate on the metal cylinder, possibly by frictional contact with the PVC and the metal airfoil.
8. An electrical field mill can be used to measure the electrical field of a body placed in the seeded vortex flow.
9. The electrical field of the wooden cylinder increased with an increase in the wind tunnel speed.

VII. RECOMMENDATIONS

The purpose of continued research in this area of studying electrical charging rates in a vortex seeded with charged particulate should be related to solving or at least understanding the charge generation problem involved in helicopters.

This study has shown the complications of the charge generation process. Another particulate feed system should be developed so that the particles entering the test region are uncharged or at least a sample of the particles would show a net charge of zero. Frictional charging seems to be the process involved. Research in the area of dielectric constants of particles encountered by hovering helicopters should be conducted, because frictional contact of particles with the aircraft is the mechanism by which the aircraft is charged. One major area of continued research should be in determining where the charge generation originates in a helicopter. This research would involve insulating various parts of the aircraft and measuring the charging rates at these various locations. For example, measure the charging rate at the rotors and compare this result with the charging rate of the helicopter body.

Concerning the charging of the cylinder in the seeded vortex, another test cylinder should be constructed so that charging rates at various locations of the test cylinder could be measured and

compared. In this manner a heavy concentration of charge in the vortex could be determined.

Continued research should be conducted for the "wetted air-foil phenomenon."

REFERENCE BIBLIOGRAPHY

1. Loeb, Leonard S., Static Electrification, Springer-Verlag, Germany, 1958, p. 215.
2. Daugherty, J., "Charge Generating and Separation Capabilities of a Trailing Vortex System," Ph.D. Dissertation, The Ohio State University, 1972.
3. Lavan, Z., and Fejer, A. A., "Luminescence in Supersonic Swirling Flow," J. Fluid Mechanics, Great Britain, Vol. 23, Part 1, 1965, pp. 173-183.
4. Loeb, Leonard B., The Basic Mechanism of Static Electrification Science, Vol. 102, No. 2658, Dec. 1945, pp. 573-576.
5. Harper, W. R., Contact and Frictional Electrification, Oxford at the Clarendon Press, 1967.
6. Whitman, V. E., Physics Review, Vol. 28, 1287, 1926.
7. Kunkel, W. B., Journal of Applied Physics, 21, 833, 1950.
8. Born, Gerard J. and Durbin, Enoch J., "An Investigation of Electrical Charging and Discharging of Aircraft in Flight," Dept. of Aeronautical Engineering, Instrumentations and Control Laboratories, Princeton University, Report No. 593, Dec. 1961, p. 11.
9. Rogers, M. E. and Minihan, E. B., "Interim Report on Investigation of Static Buildup on Helicopter."
10. Andrews, T. R. and Farret, R. H., "Evaluation of an Active Electrostatic Discharger Mounted on the Engine Exhaust of a Helicopter," Royal Aircraft Establishment, Technical Report 71219, 1971.
11. Soo, S. L., Fluid Dynamics of Multiphase Systems, Blaisdell Publishing Co., Walthorn, Massachusetts, 1967.
12. Diller, K. R., "Design and Calibration of a Low Speed Wind Tunnel," Thesis, The Ohio State University, 1966.
13. Doebelin, E. O., Measurement Systems Application and Design, McGraw-Hill Book Company, New York, 1966.

14. Evans, J. E., "The Design, Test and Evaluation of an Electrical Field Meter, Commonly Referred to as a Field Mill," Thesis, The Ohio State University, 1971.
15. Kraus, J. D., Electromagnetics, McGraw-Hill Book Company, Inc., New York, 1953, pp. 1-67.
16. Velkoff, H. R., Professor of Mechanical Engineering at The Ohio State University, 1972.

APPENDIX I

Wind Tunnel Calibration Data

Calibration of the wind tunnel was conducted by Diller (12). Figure 30 gives the wind tunnel velocity as a function of static pressure drop. Table IX indicates velocity correction factors for non-standard ambient pressure and temperature.

Figure 30

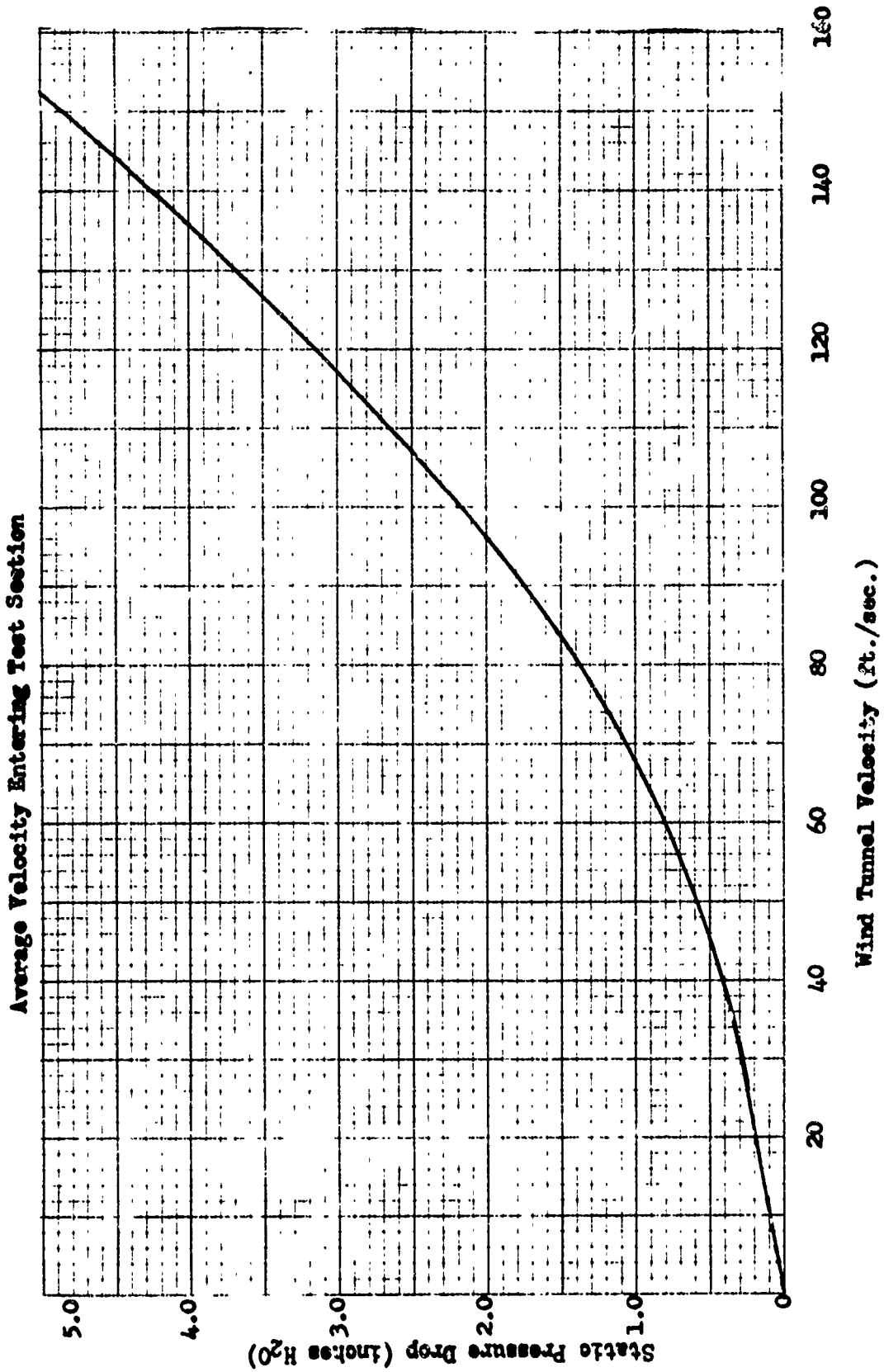


Table IX

Velocity Correction Factors for Non-standard Ambient
Pressure and Temperature

P_{AMB} (in. Hg)	K_p	T_{AMB} (F°)	K_T
29.00	1.017	55	0.965
29.20	1.013	60	0.976
29.40	1.009	65	0.988
29.60	1.006	70	1.000
29.80	1.002	75	1.015
29.921	1.000	80	1.023
30.00	0.999	85	1.035
30.20	0.995		
30.40	0.992		
30.60	0.989		
30.80	0.986		
31.00	0.983		

APPENDIX II

Poly-Vinyl-Chloride Information

Table X gives the physical properties of PVC. Results of a sieve analysis performed by Daugherty (2) are shown in Table XI.

Table X
Physical Properties of Poly-Vinyl-Chloride (PVC)

Sp. Gr. (resin)	1.4
Sp. Viscosity	0.25 - 0.55
Bulk density	0.47 - 0.58 gm./cc
Vol. resistivity	10^{14} chm./cm.
Thermal cond.	1.3 BTU/ft. - °F
Dielectric constant	3.7
Specific Heat	0.25 cal./gm. - °C

Table XI
PVC Sieve Analysis Results

Sieve Size (Microns)	<u>Supplied Distribution</u> <u>% Retained</u>			<u>Measured Distribution</u> <u>% Retained</u>	
	Test #1	#2	#3	Test #1	#2
420				.45	2
250		Trace		69.50	55
210		1			
177	0		0	11.40	21.6
149	9	41	31	16.25	19.0
105	45	40	49	1.10	2.1
100	15	6	8		
74	12	3	5	0.19	
50	19	9	7	1.08	.3

APPENDIX III

Photographs and Wiring Diagram of Experimental Set-Up

The following figures are shown in this Appendix:

<u>Figure</u>	<u>Description</u>
31A	Air Speed Adjustment Doors
31B	Particle Hopper and Nozzle
32A	Inflated Filter Bag
32B	Differential Airfoils
33A	Metal Cylinder in Holding Fixture
33B	Wooden Cylinder in Holding Fixture
34A	Electrical Field Mill and Wooden Cylinder
34B	Electrical Field Mill Inserted in Wooden Cylinder
35	Electrical Equipment Set-up
36	Wiring Diagram of Test Instrumentation

Figure 31A
Air Speed Adjustment Doors

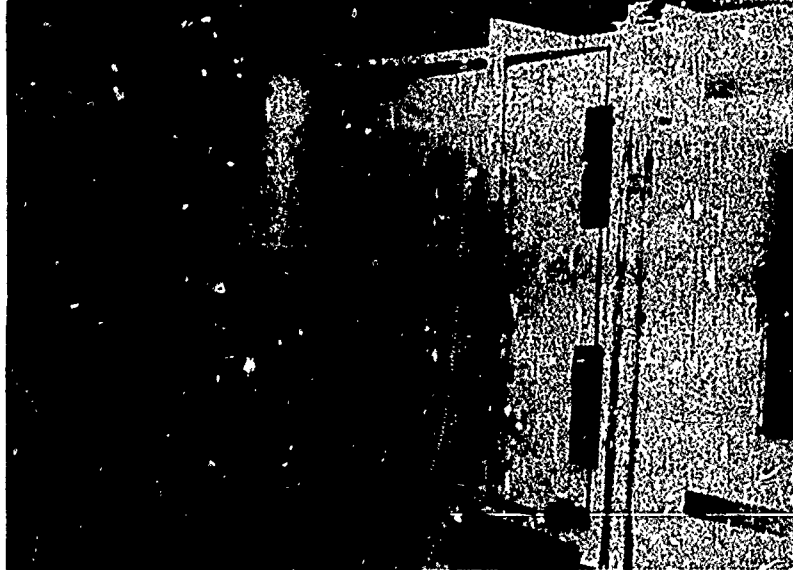


Figure 31B
Particle Hopper and Nozzle

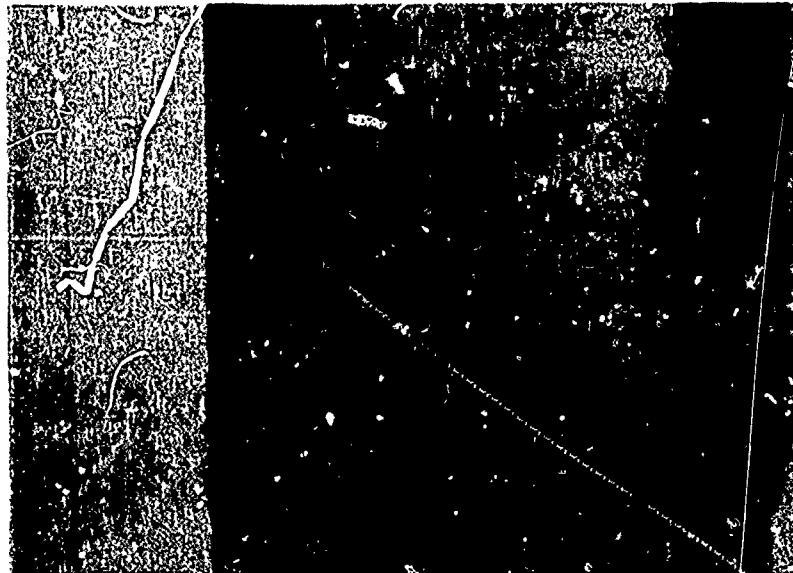


Figure 32A
Inflated Filter Bag



Figure 32B
Differential Airfoils

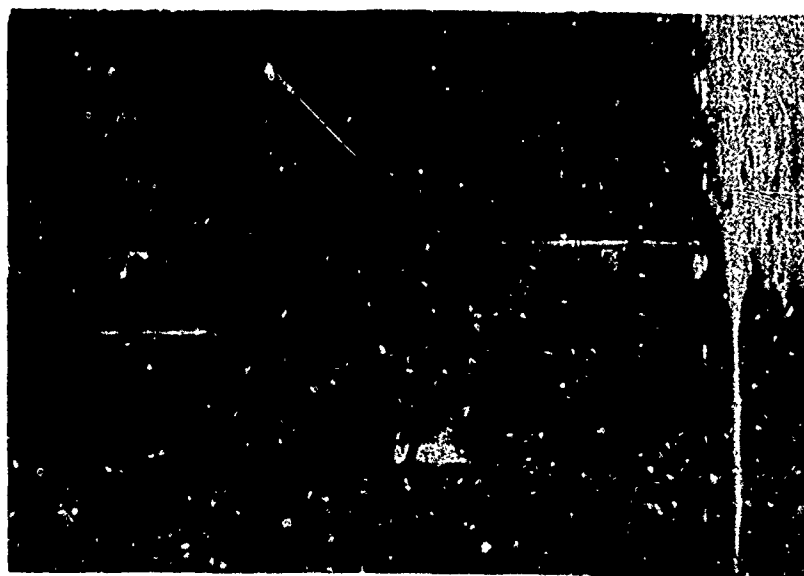


Figure 33A

Metal Cylinder in Holding Fixture
at Centerline Position

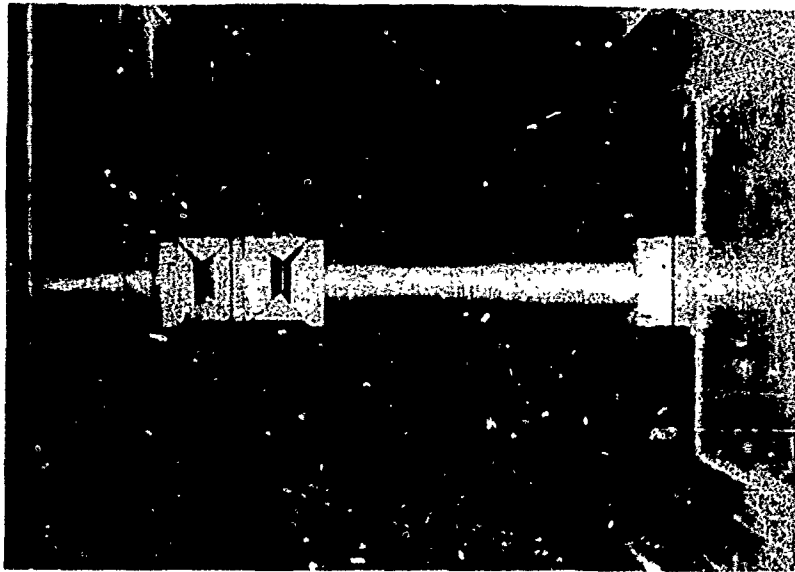


Figure 33B

Wooden Cylinder in Holding Fixture
With Electrical Field Mill

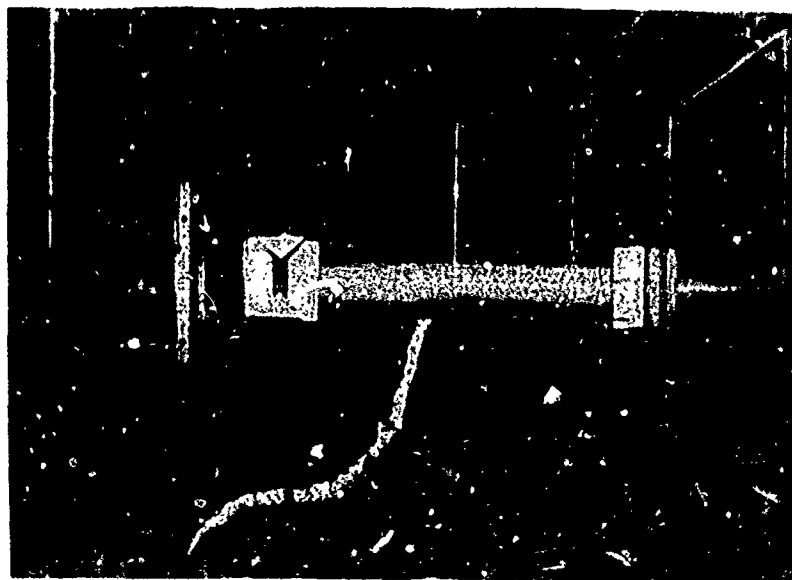


Figure 34A

Electrical Field Mill and Wooden Cylinder

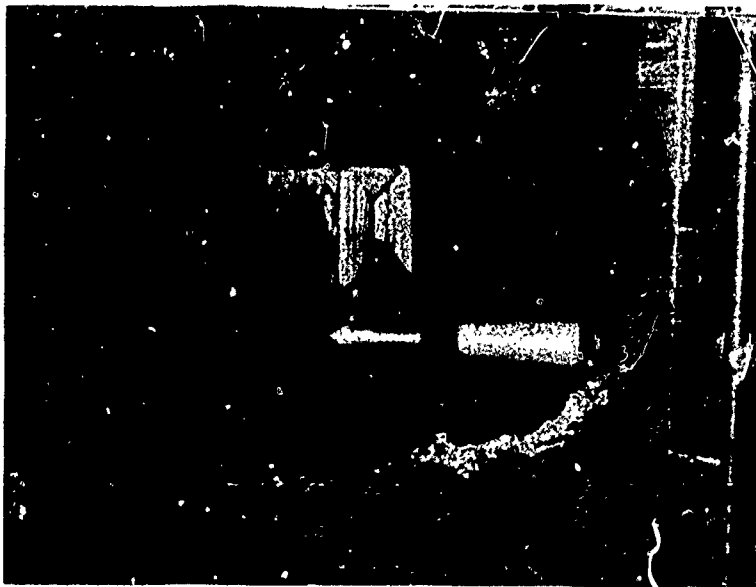


Figure 34B

Electric Field Mill inserted in Wooden Cylinder

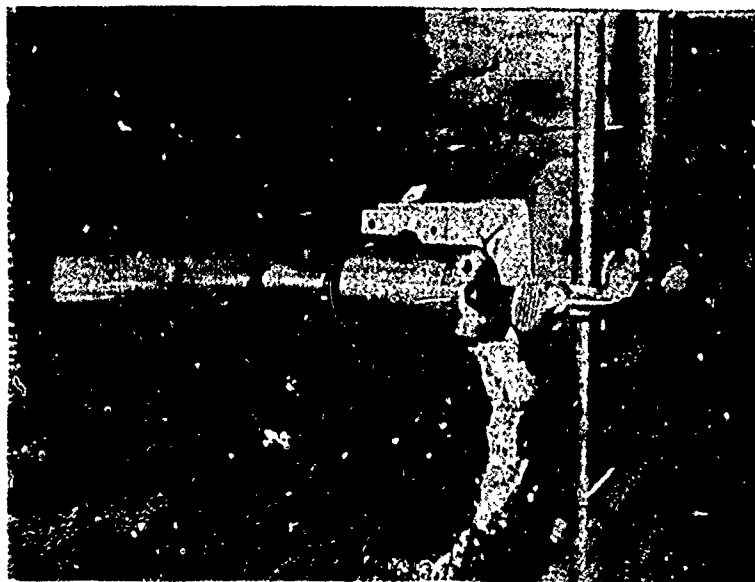


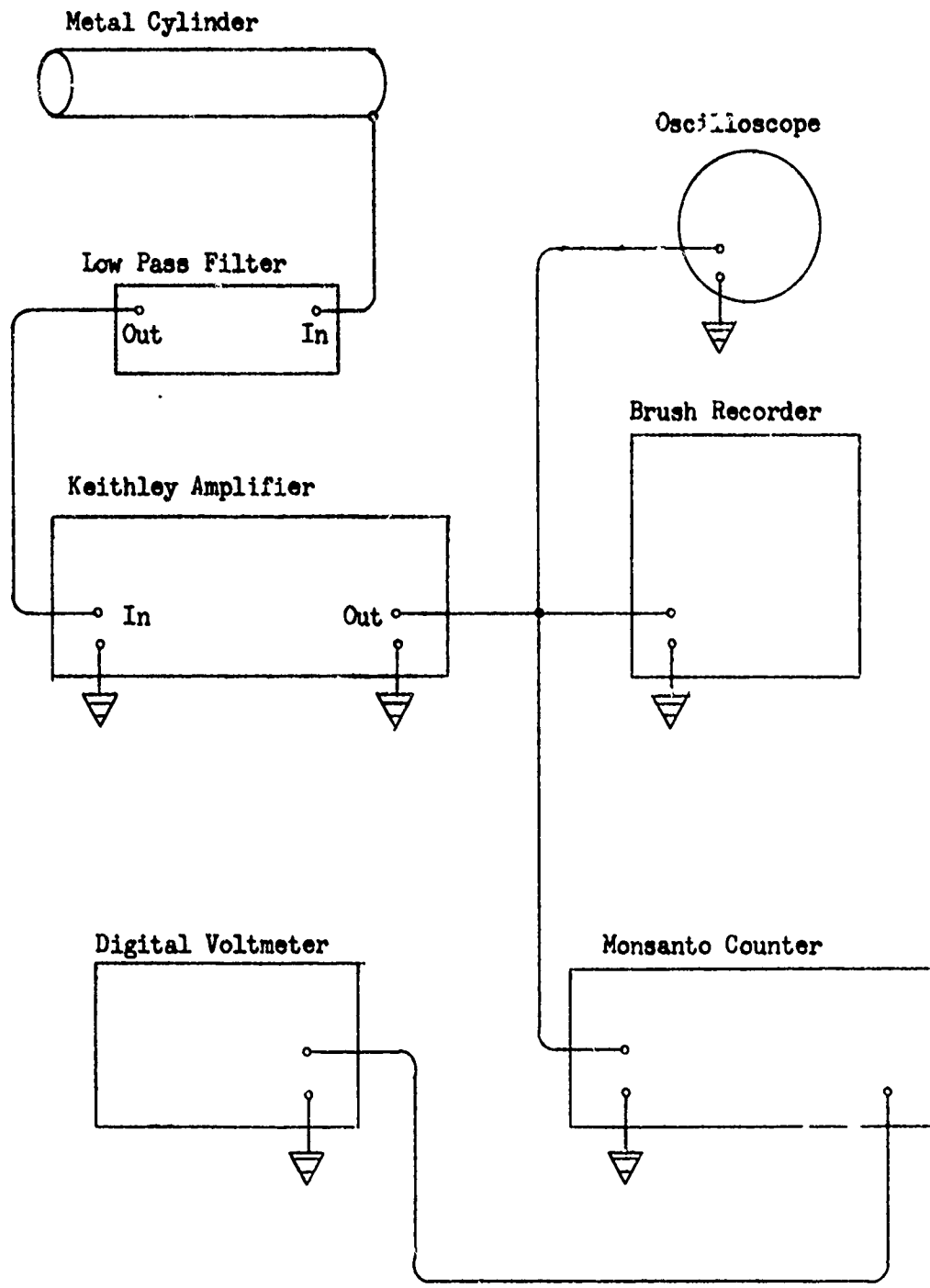
Figure 35
Electrical Equipment Set-Up



- 1 - Brush Recorder
- 2 - Oscilloscope
- 3 - Low Pass Filter
- 4 - Keithley Amplifier
- 5 - Digital Voltmeter
- 6 - Monsanto Counter

Figure 36

Wiring Diagram of Test Instrumentation



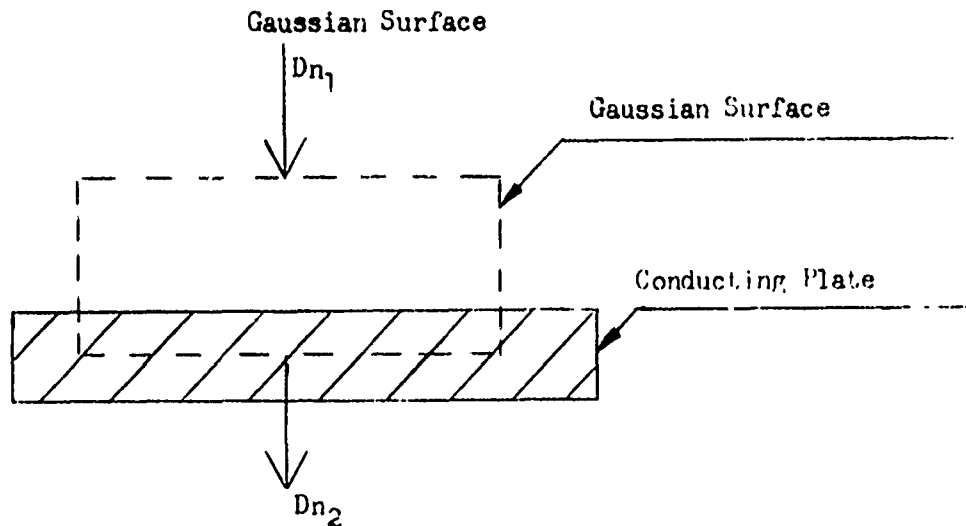
APPENDIX IV

Operation of the Electrical Field Mill.

The basic operating principle of the field mill is the alternate screening and exposing of a conductor to an electric field, thereby inducing an alternating current. When the induced current is applied to a high impedance, such as to the Tektronix Oscilloscope, it produces a voltage proportional to the electrical field strength.

Using the notation from Evans (14), a theoretical analysis of the electrical field near a conductor can be determined. Gauss's law for an electrical field (15) states that "the surface integral of the normal component of the electrical flux density, \bar{D} , over any closed surface equals the charge enclosed". Figure 37 shows a Gaussian surface by dotted lines that is bounded on the upper surface by air and the lower surface by a conducting plate.

Figure 37



The following notation is used:

D_{n_1} = average inward normal electric flux density in air

D_{n_2} = average outward normal electric flux density in the conductor

ρ_s = surface charge on the plate

\bar{E} = the electrical field

ϵ = permittivity

Q = net charge

The electric flux density is defined as $\bar{D} = \epsilon \bar{E}$.

Now, taking the integral over the Gaussian surface gives the following result:

$$\int \bar{D} \cdot d\bar{s} = Q$$

$$D_{n_2} - D_{n_1} = \rho_s$$

Although in a conductor the electric field and electric flux density are zero, so $D_{n_2} = 0$ which leads to:

$$-D_{n_1} = \rho_s$$

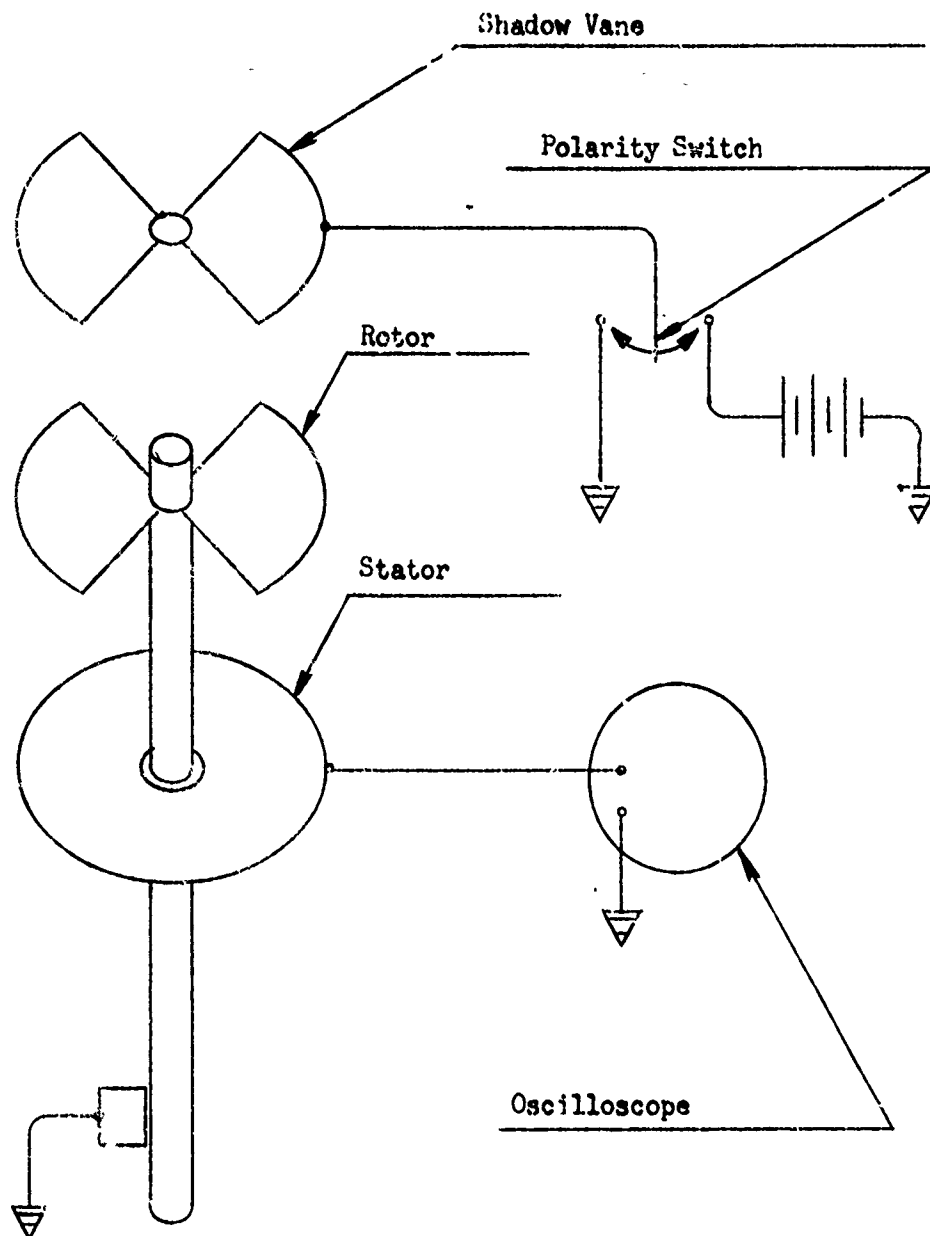
As stated earlier, the electric flux density, $\bar{D} = \epsilon \bar{E}$. This implies that the surface charge is proportioned to the electric field \bar{E} .

The electric field induces a surface charge on the conductor equal in magnitude to the normal component of the electric flux density but opposite in sign.

Evans' (14) field mill consisted of a three vane head section as shown in Figure 38. The rotor was propelled by a small electric motor in the field mill housing. When the vanes of the shadow vane and rotor were lined up with one another, the electric field lines could be detected by the stator, but as the grounded rotor was rotated, it would block off the electric field lines going to the stator. As presented earlier the electric field lines induced a surface charge on the conducting stator. As the electric field was alternately exposed and covered by the motion of the rotor, the surface charge on the stator alternately changed from zero to some magnitude proportional to the electrical field. The output from the stator revealed a sinusoidal voltage proportional to the electrical field being measured.

The polarity of an electrical field can be determined by use of the shadow vane in this head section. When a potential was applied to the shadow vane, an electrical field was set up between the shadow vane and the stator. The resulting voltage output from the stator, which was zero when the shadow vane was grounded, was the reference voltage level. Therefore, when an unknown electric field to be measured had the same polarity as the applied electric field to the shadow vane, the reference voltage was raised. A decrease in the signal voltage resulted when compared to the voltage obtained in the case where the shadow vane was grounded. The opposite occurred when an unknown field of opposite polarity was presented.

Figure 38
Field Mill Head Section

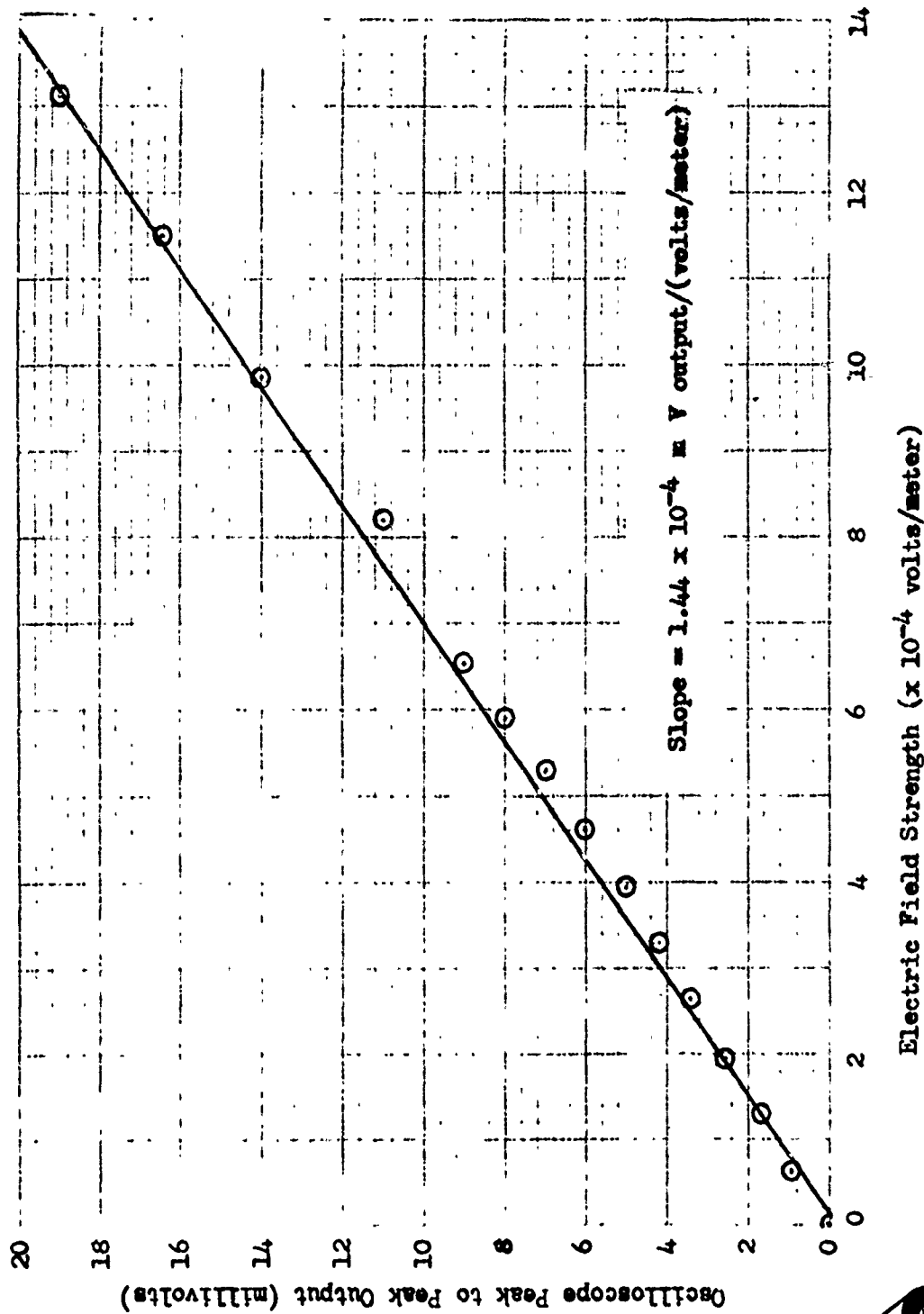


The reference voltage was lowered and the signal voltage was greater than when the shadow vane was grounded.

Some initial testing of Evans' field mill (14) in the wind tunnel with seeded flow indicated much noise in the signal produced by particles in the flow impinging on the exposed stator. To remedy the situation, Evans placed a conducting deflecting cone above the shadow vane. This alteration reduced the electrical field although fringe effects from the cone were still detected by the stator and thus gave an indication of the electrical field present.

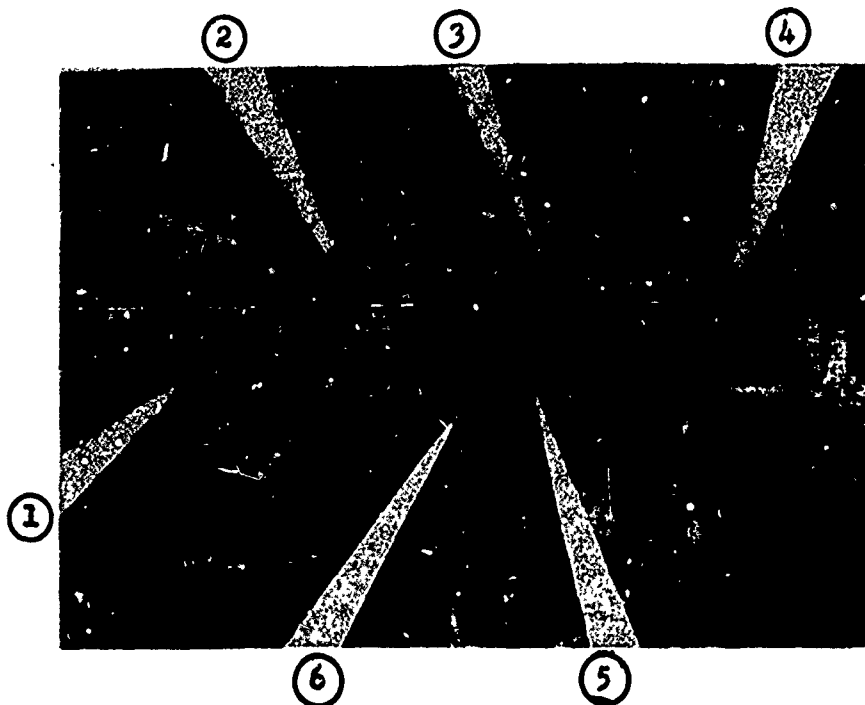
The electrical field mill was calibrated by placing it in a uniform electric field. The electric field was produced by separating two three foot square aluminum plates one foot apart by wooden supports, and applying a potential across the plates by a high voltage D.C. power supply. To reduce electric field fringe effects and keep the field mill as close to the grounded plate as possible, a small hole was bored in the center of the grounded plate so that the head vane section of the field mill just protruded through the hole. Figure 39 shows the calibration curve, which indicates a straight line function relating peak to peak voltage output to the electrical field. Figure 40 shows a photograph of the calibration set-up for the field mill.

Figure 39
Electric Field Mill Calibration



Reproduced from
best available copy. C

Figure 40
Field Mill Calibration Set-Up



- 1 - High Voltage Supply
- 2 - Oscilloscope
- 3 - Test Capacitor
- 4 - Electrostatic Voltmeter
- 5 - Electric Field Mill
- 6 - Polarity Switch and Batteries